# Measurement of the charge asymmetry in top quark pair decay in dilepton (e,$\mu$) channel in pp collision data at $\sqrt{s} = 7$ TeV using the ATLAS detector

Donya MashaallahPoor

Supervisor: Else Lytken


LUND UNIVERSITY

Department Of Physics
Particle Physics Division
Lund University
October 2014

# Innehåll

# 1 Public Abstract

Det vi idag kallar materia och som ligger till grund för hela vårt universum är egentligen en kombination av fundamentala partiklar och deras växelverkan. Detta sammanfattas i Standard Modellen (SM).

Toppkvarken är modellens tyngsta partikel och behöver en process med väldigt stor energi för att kunna skapas. Toppkvarken kan experimentellt observeras antingen ensam eller i form av ett par (en toppkvark och en anti-toppkvark). När den produceras i par finns det en möjlighet att studera laddningsasymmetri (ämnet för denna avhandling), vilket skulle medföra ny fysik som går utanför SM. Indikationer på sådan laddningsasymmetri i toppkvarkpar observerades för första gången i CDF-experimentet vid Tevatronen där protoner och antiprotoner kolliderar. I sådana kollisioner antar man att den producerade toppkvarken sänds ut i protonens riktning och att den producerade anti-toppkvarken sänds ut i anti-protonens riktning. Toppkvarkarnas masscentrum kan därvidlag antingen röra sig i protonens eller i antiprotonens riktning och på så vis medföra en asymmetri i laddningen hos de slutligen producerade partiklarna.

I denna avhandling mäts laddningsasymmetrin med hjälp av ATLAS-detektorn vid LHC-kolliderarен på CERN, där båda de kolliderande partiklarna är protoner. Det finns två sätt att mäta laddningsasymmetrin i ATLAS-experimentet; toppkvark-baserat eller lepton-baserat. Eftersom någon ursprunglig anti-proton saknas, kan man här inte bestämma anti-toppkvarkens riktning, vilket gör en laddningsasymmetrimätning baserad på toppkvarken ytterst komplicerad. Ett värde på laddningsasymmetrin kan emellertid erhållas:

$$A_C^{t\bar{t}} = -0.036 \pm 0.014$$

Laddningsasymmetrimätning baserad på leptoner är en vanligtvis använd metod i proton-proton kollisioner. Den använder sig av laddningsasymmetrin hos de leptoner som bildas då toppkvarkarna sönderfaller, som i denna analys är en elektron och en myon. Det erhållna värdet på laddningsasymmetrin blir här:

$$A_C^{l\bar{l}} = 0.007 \pm 0.014$$

Den slutliga jämförelsen mellan det erhållna värdet och resultat från simuleringar, pekar mot att ingen ny fysik, som går utanför SM, behövs för att förklara resultaten.

# 2 Introduction

Particle physics is the science which deals with the basic constituents of matter and their interactions with the different forces of nature. Since these constituents need a very high energy to be taken apart, it is also known as high energy physics.
A very quick view of the history of physics of matter, makes it obvious that the belief of basic constituents of matter was formed through the $19^{th}$ century. In the late $19^{th}$, the discovery of the electrons by the British physicist, J.J.Thomson in 1896 was a manifest evidence of disintegratibility of atom. At the same year, the discovery of radioactivity by Wilhelm Roentgen, who discovered the X-ray, and later studies in $20^{th}$ century about radiation and the types of radioactivity, proved that the universe consists of the fundamental particles. This proof opened the window to the science of particle physics. The result of all these experiments and studies created one of the most important theories of $20^{th}$ century "Standard Model"of particle physics which is the bases of the most particle physics experiments and is still under study.

## 2.1 *The Standard Model*

The Standard Model, as one of the most successful particle physics theories in adaptation with the experiments, explains almost all the known fundamental particles and natural forces except gravity. Fig.1 shows the table of all known fundamental particles.

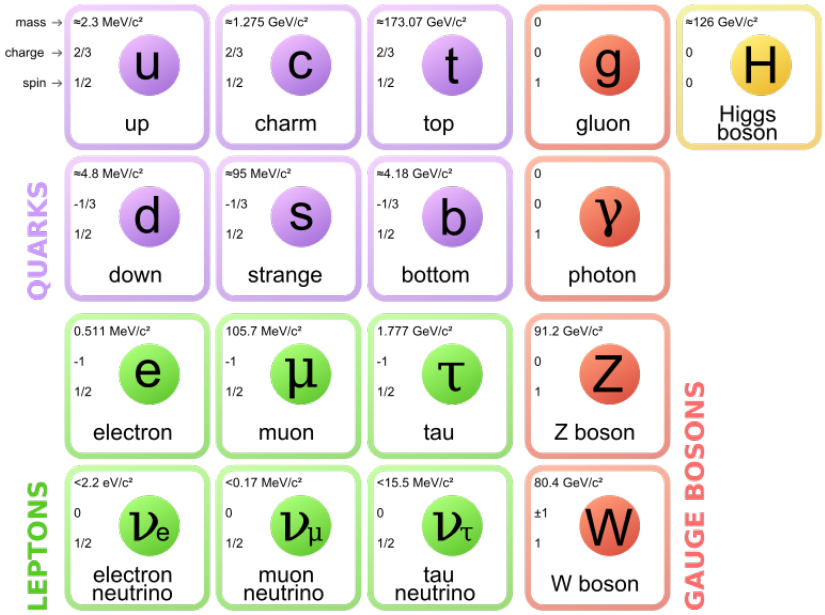


Figur 1: Standard model table[1]

In this model, particles are divided into two main groups of *fermions* and *bosons*. All the particles with half-integer spin are in the group of *fermions*. Based on the type of their interactions and charges, this group is divided into two classes of *leptons* and *quarks*. All these particles obey *Fermi-Dirac statistics*[2] which is based on the *Pauli exclusion principle*[3]. By reviewing the fermions in more details, the classes of quarks and leptons can be studied separately in three generations of:

$$\begin{pmatrix} u \\ d \end{pmatrix} \begin{pmatrix} c \\ s \end{pmatrix} \begin{pmatrix} t \\ b \end{pmatrix}$$

$$\begin{pmatrix} \nu_e \\ e \end{pmatrix} \begin{pmatrix} \nu_\mu \\ \mu \end{pmatrix} \begin{pmatrix} \nu_\tau \\ \tau \end{pmatrix}$$

Some general information about fermions like mass, charge and spin are shown in Fig.1. They are the physical properties of the particles except spin. Spin is the intrinsic form of angular momentum. The existence of spin is concluded from experiments when the angular momentum is not explainable just by the orbital angular momentum in the experiments. Quarks have fractional charge of + $\frac{2}{3}$ and -$\frac{1}{3}$ and leptons have charge of -1 and zero. Moreover, quarks are specified by a special quantum property that is named *color* and comes in three types: red, blue and green. Color is the most important difference between leptons and quarks. Basically as quarks carry the color as well as charge, it is possible for them to have interaction with all the forces when leptons due to not carrying the color flavor, cannot be in any combination of particles which is hold by the strong force.

Bosons obey *Bose-Einstein principle*, it means there is no restriction for identical bosons to be produced in a same quantum state. It has been proved in standard model that the force transportation between particles is done by bosons. Thus, they are called *force carriers*. For example, the electromagnetic force is carried by photons and the strong force is carried by gluons. Here, the properties of natural forces and their related force carriers shown in the table below:

| | **Strong** | **Electromagnetic** | **Weak** | **Gravity** |
|---|---|---|---|---|
| **Mediator** | gluon | Photons | $W^+, W^-, Z^0$ | Graviton |
| **Mass** | 0 | $W^-, W^+ \sim 80GeV$, $Z^0 \sim 90GeV$ | 0 | 0 |
| **Range** | $\sim 10^{-15}$ | $\infty$ | $\sim 10^{-18}$ | $\infty$ |
| **Fermions affected** | Color charged | electrically charged | all | all with mass |
| **Relative strength** | 1 | $\sim 10^{-2}$ | $\sim 10^{-6}$ | $\sim 10^{-39}$ |

Tabell 1: Table of forces, force-carriers and their properties. All the last row quantities in the table are the relative strength of the forces to one.[4].

Amongst all the forces, it is just gravity that has not been accounted by the standard model yet. If we consider the strong force as the most strongest force, the gravity with the relative strength of $10^{-39}$ to the strong force is the weakest force of the nature. Being very weak in comparison to the other forces is one of the reasons of its incompatibility with the quantum scale in quantum theory, although it works well under a classical theory or general relativity.

## 2.2 *Electroweak Theory*

All the weak, electromagnetic and strong forces have the same mathematical framework in the standard model. This framework is defined in the *gauge symmetry* form of:

$$SU(3)_C \times SU(2)_L \times U(1)_Y \tag{1}$$

Eq.1 contains two groups. One is $SU(3)_C$, which comes from the *Quantum Chromodynamics* (QCD) and will be explained more in next section. The subscript C here refers to Color charge. The second group is the *electroweak theory* in form of $SU(2)_L \times U(1)_Y$. L for *weak isospin* and Y represents *weak hypercharge*. The electroweak theory is the unification of the electromagnetic and weak interactions based on the theory of Glashow-Salam-Weinberg (GSW). $SU(2)_L$ refers to the weak interaction in this combination and W-boson in three forms of $W^+$, $W^0$ and $W^-$ are the force carriers based on the GSW theory. Another term $U(1)_Y$ belongs to the electromagnetic interaction and for unifying these two interactions this term should also have a force carrier which is called $B$ boson. The B-boson and $W^0$-boson later combine based on the spontaneous symmetry breaking and form two bosons of $Z^0$-boson and the photon($\gamma$) which are known as the mediators of the weak force and electromagnetic force in the Standard Model. To keep the unification of the electromagnetic and weak forces and the symmetry between these two, all the mentioned bosons should be massless while later in the experiments, it was discovered that Z and W-boson have considerable masses while the other two bosons, the photon and the gluon, still have zero mass. Giving mass to the bosons of the weak force, through the *Higgs Mechanism*, spontaneously breaks the symmetry of the electroweak force.

## 2.3 *QCD*

Quantum Chromodynamics (QCD) the theory of the strong interaction and the color charge. It explains the color charge as the quantum number of the quarks and gluons. It shows that gluons are emitted and collected by the quarks in a strong interaction and it can change the color of the quarks. Since the gluons are color-charged, combinations of gluons also exist and they can interact together and make change in quarks and anti-quarks. There are eight different colored gluons. QCD explains that the strong force can interact just with the particles that are charged by colors. Based on this fact and existence of color flavored gluons, not just quarks but gluons can interact

with themselves. Gluons are the only force carriers which have interaction with each other due to carrying color.

## 2.4 *The CKM Matrix*

The *Cabibbo-Kobayashi-Maskawa*, or CKM matrix, is another considerable topic in the SM that is focused on the weak decays of quarks and hadrons. In principle, the CKM matrix is a bridge between the weak eigenstates $(d', s', b')$ with their corresponding mass eigenstates (d, s, b). It is shown in the Eq.2.

$$\begin{pmatrix} d' \\ s' \\ b' \end{pmatrix} = \begin{pmatrix} V_{ud} & V_{us} & V_{ub} \\ V_{cd} & V_{cs} & V_{cb} \\ V_{td} & V_{ts} & V_{tb} \end{pmatrix} \begin{pmatrix} d \\ s \\ b \end{pmatrix} \equiv V_{CKM} \begin{pmatrix} d \\ s \\ b \end{pmatrix} \tag{2}$$

The numerical version of the matrix looks like:

$$|V_{CKM}| = \begin{pmatrix} 0.974280.00015 & 0.22530.0007 & 0.00347^{+0.00016}_{0.00012} \\ 0.22520.0007 & 0.97345^{+0.00015}_{0.00016} & 0.0410^{+0.0011}_{0.0007} \\ when 0.00862^{+0.00026}_{0.00020} & 0.0403^{+0.0011}_{0.0007} & 0.999152^{+0.000030}_{0.000045} \end{pmatrix}^{[6]} \tag{3}$$

In a quick view it is obvious that the maximum values appears when the transition is within the same family. Basically, the CKM matrix shows the transition probability between one type of quark to another one. As it is shown in the Eq.3, $V_{tb}$ has the highest probability of transition from top quark to b-quark which is considerable.

# 3 The Top Quark

The top quark as the heaviest known fundamental particle was discovered in 1995 at one of the world's highest energy accelerators, the Tevatron Collider at FermiLab in the United States. In this accelerator with two major experiments, D0 and CDF, colliding proton and anti-proton beams led to the top quark discovery[7]. The top quark as one of the special particles in the Standard Model was discovered in pair and has motivated the physicists to study this particle in more details.

The top quark is from the third generation of quarks with the short lifetime of:

$$\tau \sim 5 \times 10^{-25} s.^{[8]} \tag{4}$$

This lifetime is shorter than the time it needs to travel the distance between its produced point to the detectors. It is even shorter than $3 \times 10^{-24}$s[8] which is the time a top quark needs to form a QCD bound state and interact with other quarks to form a hadron. Thus, it decays through electroweak interaction although it interacts with both strong and electroweak forces.
The top quark with a mass of $173.07 \pm 0.52$GeV[9] is also heavier than W and Z-bosons which are force carriers of the electroweak forces. Thus, it is comparable with the electroweak symmetry breaking scale and as it is

displayed in Fig.2, it is one of the important particles that participates in the Higgs boson production processes.

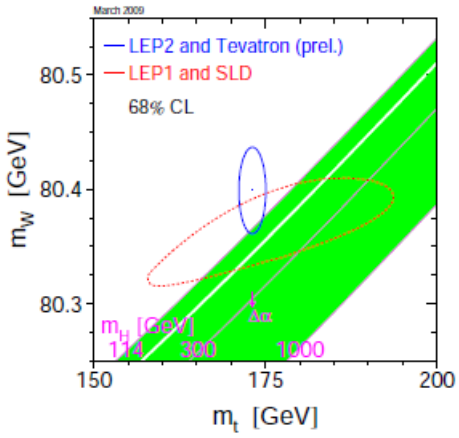


Figur 2: Combined constraints on the Higgs boson mass.[11]

Since the top quark cannot produce hadrons, it lives like a free particle in its extreme short lifetime. The process of producing the top quark includes the b-quark and the b-jets. Hence, it increases the possibility of observing and studying *bare-quarks*. Another importance of studying this fermion is searching for *flavor-changing neutral-current* (FCNC) event. FCNC could happen in the top quark decay processes and involves producing same-sign top quark pairs[8]. The top quark is important as a background for Super Symmetry (SUSY) and for many new models as well. The other aspect of the top quark events which manifests this quark from the other particles and is the main part of this thesis, is the potential for the charge asymmetry in the top quark pairs in their productions. Observing the charge asymmetry provides a new window for beyond the Standard Model.

## 3.1 *The Top Quark Production*

As the top quark is a very heavy particle it can just be produced in the high energy events. The high energy process is modeled with the *parton model*. According to this model, when two hadrons collide, the collision occurs between the individual quarks and it does not involve the whole hadrons. The involved part which is called *parton* is not just the valence quarks but

sea quarks and gluons as well. The other quarks in hadrons which do not participate in this process, will also hadronise into other hadrons to make the background particles. In Fig.3, two protons collide and a parton from

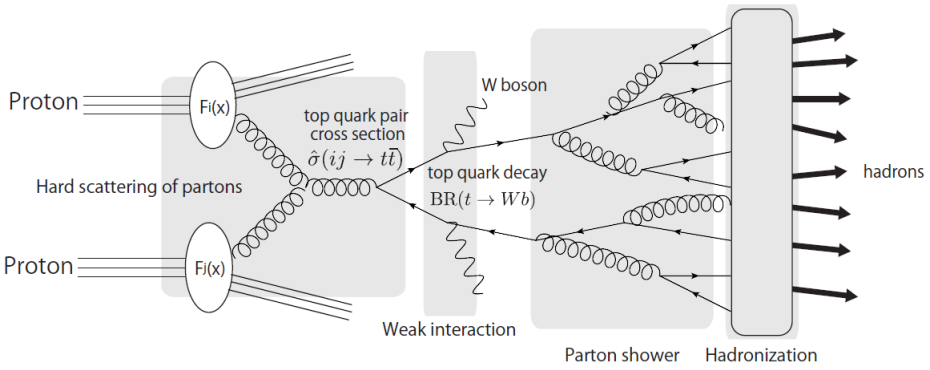


Figur 3: A scheme of physics processes in the top quark production and decay[12]

each, interacts. Due to many parallel interactions and large number of produced particles, components of parton has not been distinguished clearly up to now. Thus, peturbative QCD cannot calculate this variable precisely. In this technique for recognizing a particle, different related terms of a particle are calculated but the strong interaction scale, the coupling constant ($\alpha_s$), is so small in this theory and is not calculable accurately.

The information about the type of scattering can be obtained by the cross-section of the partons. Finding the cross-section is possible by using the *Parton Distribution Function*(PDF), $f_i(x_i, \mu^2)$, of each proton in the collision. The total cross-section in this method is calculated by:

$$\sigma_{pp\to t\bar{t}}(s, m_t) = \sum_{i,j=q,\bar{q},g} \int dx_i dx_j f_i(x_i, \mu_f^2) f_j(x_j, \mu_f^2).\sigma_{ij\to t\bar{t}}(s, m_t, \mu_f, \mu_r, \alpha_s)^{[8]} \tag{5}$$

where $x_i$ is the fraction of the mother proton momentum carried by quark i, $\mu^2$ is the event renormalization scale, $s$ is the center of mass energy of the partons interaction, $m_t$ is the top quark mass and $\alpha_s$ is the strong coupling constant. The latter variable, based on the level of order of the particle in the process would have different values like $\alpha_s^2$, $\alpha_s^3$. The power of the constant

represents the scale of high energy in the process.

Based on the type of parton interaction, the top quarks can be produced in single or pair forms. Basically, the top quark pair comes out from the strong interaction and through two main processes: *quark and anti-quark annihilation* and *gluon-gluon fusion*. Feynman diagrams in Fig.4 describe the simple form of these processes.

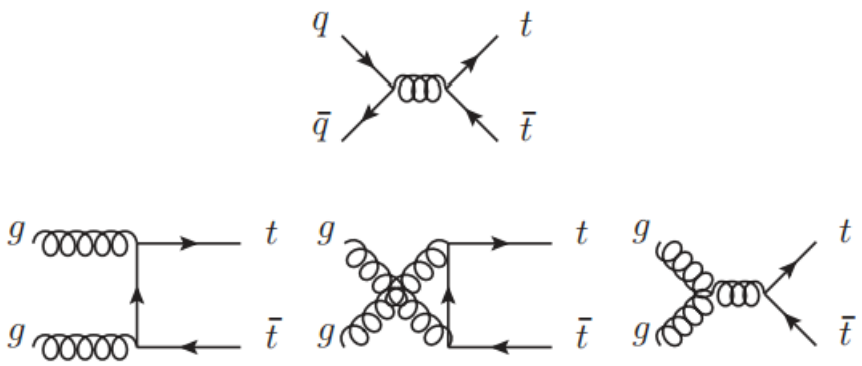


Figur 4: Feynman diagrams for $t\bar{t}$ production at leading order QCD. Top: $q\bar{q}$-annihilation. Down: gluon-gluon fusion.[8]

In the $q\bar{q}$ annihilation, a quark and an anti-quark annihilate into a gluon and produce a top quark pair. In the gluon-gluon fusion, this process is achieved by the interaction between gluons. The probability of each of these processes to happen depends on the beam properties like center of mass energy of the beams that affects the cross-section and changes the priority of the processes. At Tevatron with the low energy scale of $\sqrt{s} = 1.96TeV$, where the the collided beam is proton and anti-proton, there are a large number of anti-quarks as well as quarks. The process mostly occurs with the valence quarks and they hold higher momentum fractions. This increases the probability of the $q\bar{q}$ annihilation processes. At the LHC with the beam energy of $\sqrt{s} = 7TeV$, the parton consists of sea quarks and gluons as well as valence quarks. Hence they carry the lower momentum fraction of the beam and there are more gluon-gluon fusion events produced than $q\bar{q}$ annihilation. This comparison is shown clearly in Fig.5.

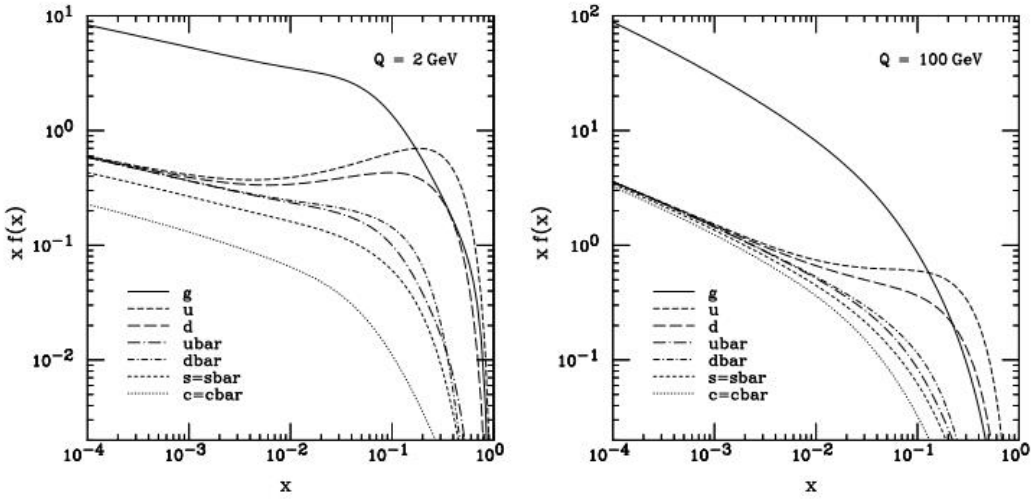


Figur 5: Overview of the CTEQ6M parton distribution functions[13]. Left(Q = 2 GeV): The dominance of the valence quarks increases in the nucleon at lower $xf(x)$ and they carry high fraction of momentum $x$. Thus the top quark pair is produced under $q\bar{q}$ annihilation processes. Right(Q = 100 GeV): The number of sea quarks increases in the parton at lower $xf(x)$ and they carry low fraction of momentum $x$. The remained part of energy is carried by the gluons. Hence, the gluon-gluon fusion is dominant.

The other form of the top quark production, single top quark, is a result of the weak interaction. There are three main channels for single top quark production which are *tW-channel*, *s-channel*, *t-channel*. Fig.6 shows Feynman diagrams of all these channels in more details.

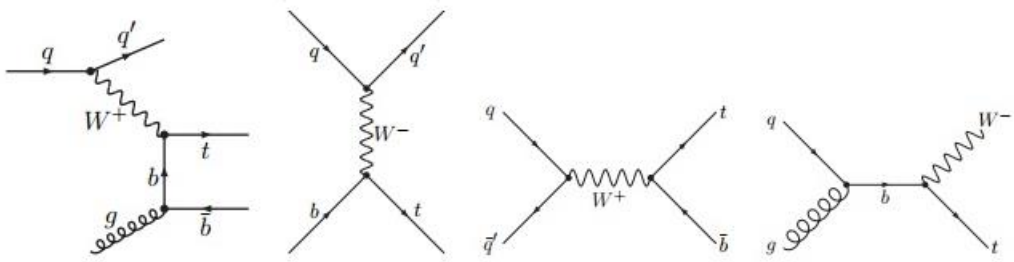


Figur 6: Single top quarks channels. From left; 1st and 2nd: t-channel, s-channel, wt-channel.[14].

The study of single top quark has also its own importance. For instance, it has a key role in measuring the CKM matrix element, $V_{tb}$. Furthermore, the single top quark is produced via W-boson and there is a straightforward relation between producing a single top quark and the $W_{tb}$ coupling. Hence, the single top quark production processes as well as top pair productions, can have a remarkable place in studying the standard model deviation.

## 3.2 *The Top Quark Decay*

The short lifetime of the top quark does not let this quark to get involved with complicated interactions of color charged particles. Having no hadronization possibility makes the top quark decaying through a weak decay and to the lighter quarks. The absence of hadronization allows the top quark to be

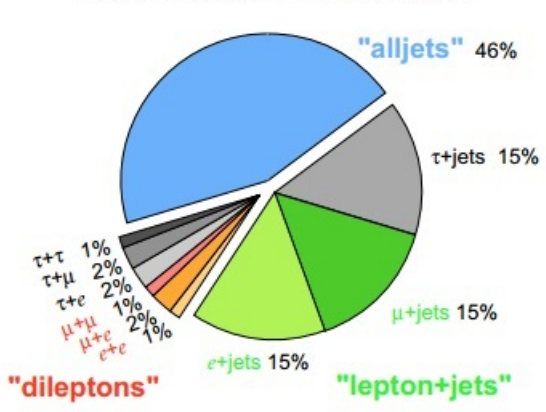


Figur 7: Top quark pair branching fractions[15].

traced more simply. It is possible due to the transmission of the top quark spin information to the decay products[12]. It implies that the top quark spin information does not change and it transfers to the daughter particles. Thus, by gathering the information of the produced daughters, tracing the top quark becomes possible. According to the CKM matrix values, the top quark with very high probability decays to b-quark and W-boson. The information of tracing is gathered by the produced particles from the W-boson decay. The W-boson has three decay modes. They are also is shown in the Fig.7.

**Full hadronic decay or "all jets" decay** is when both W-bosons decay into $q\bar{q}$ and these quarks are from lighter quarks. $t\bar{t} \rightarrow W^{+}b\, W^{-}\bar{b} \rightarrow q\bar{q}\ q\bar{q} + (b)jets \rightarrow jets$

**Semi-leptonic or "lepton+jets" decay** is when one W-boson decays to $q\bar{q}$ and the other one decays into one lepton and one lepton-neutrino. $t\bar{t} \rightarrow W^{+}bW^{-}\bar{b} \rightarrow q\bar{q}\ l^{-}\bar{\nu}_{l} + (b)jets$

**Dileptonic decay** is when both W-bosons decay into one lepton and one lepton-neutrino. $t\bar{t} \rightarrow W^{+}bW^{-}\bar{b} \rightarrow l^{+}\nu_{l}\ l^{-}\bar{\nu}_{l} + (b)jets$

The last mode is studied in this thesis.

## 3.3 *The Top Quark Charge Asymmetry*

In the top quark pair decay, the center of mass of the final products might move in the direction of one of the initial beams and create an asymmetry in the charge of the final products. The reason for this asymmetry can be explained by the momentum fraction values of the partons which give rise to the products. The two partons need a new dynamics to hold the symmetry between the produced top and anti-top quarks but since this process includes a lot of light quarks, the energy transfer from partons to the new products might create an asymmetry[16]. This asymmetry, especially in collisions where particles and anti-particles collide, is measured by counting the rate of positive and negative produced charged particles in the direction of beam lines. Based on this explanation, the simple definition of asymmetry between the initial and the final radiation is obtained by:

$$Asymmetry = \frac{N^{+} - N^{-}}{N^{+} + N^{-}} \tag{6}$$

where $N^{+}$ and $N^{-}$ are the ratio of the positive and negative particles. There are different options to measure this value in the $t\bar{t}$ production in different accelerators. The *Forward-backward asymmetry*($A_{FB}$) is an option to calculate the asymmetry at the Tevatron with the CDF and D0 detectors where one beam is a proton and the other one is an anti-proton. Since at this accelerator the $t\bar{t}$ production is based on the $q\bar{q}$ annihilation process, it is supposed that top quarks mostly move in the proton beam direction and anti-top quarks move along the anti-proton beam[17].

At the LHC where both beams are protons, the gluon-gluon interaction is dominant. Hence, the initial state is symmetric and measuring forward-backward asymmetry is not as easy as at the Tevatron[18]. The charge asymmetry at the LHC, $A_C$, which is the purpose of this thesis, has two forms. One form is based on the rapidity of the top and anti-top quarks. The angular property of the top quark which is related to the beam axis is the *Rapidity* and can be calculated by:

$$y = \frac{1}{2} ln \frac{E + |p_z|c}{E - |p_z|c} \tag{7}$$

where $|p_z|$ is the momentum component along the beam axis. Now the charge asymmetry equation based on the rapidity is expressed as:

$$A_C^{t\bar{t}} = \frac{N(\Delta|y| > 0) - N(\Delta|y| < 0)}{N(\Delta|y| > 0) + N(\Delta|y| < 0)} \tag{8}$$

where $\Delta|y| = |y_t| - |y_{\bar{t}}|$ is the difference of the top and anti-top quark absolute value of rapidity. The other form of charge asymmetry is based on the polar angle between the positive and negative final charged leptons. The lepton-based formula is defined by:

$$A_C^{ll} = \frac{N(\Delta|\eta| > 0) - N(\Delta|\eta| < 0)}{N(\Delta|\eta| > 0) + N(\Delta|\eta| < 0)} \tag{9}$$

where $\eta$ represents the pseudorapidity. This value is calculated by:

$$\eta = -\ln \tan(\theta/2) \tag{10}$$

where $\theta$ is the polar angle between the vertical component of the particle momentum and the positive direction of the beam axis. $\Delta|\eta| = |\eta_{l^+}| - |\eta_{l^-}|$ is the difference of the positive and negative leptons absolute value of pseudorapidity. When the particle reaches the speed of light, the value of pseudorapidity is close to the rapidity.
In these two methods, the lepton-based asymmetry is easier, since leptons are the final products which are observed directly by the detectors. Thus, the reconstruction of the top quark pair final state is not needed. Although, due to not focusing on the main particles (top quark and top anti-quark) for measuring the asymmetry, it might not show a very accurate result.

# 4 The ATLAS Detector

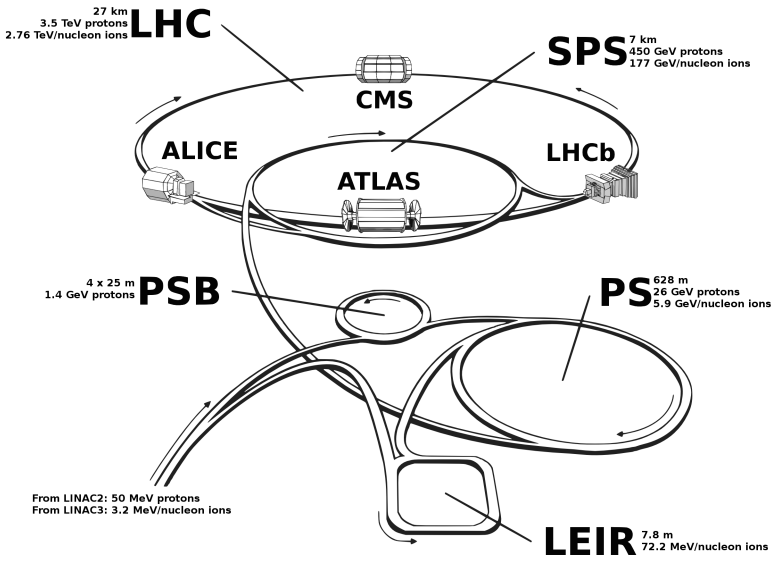


Figur 8: The schematic view of CERN ring and different accelerators.

The Large Hadron Collider (LHC) at CERN is the largest and the most powerful collider in the world which is located in Geneva, Switzerland. The schematic view of the accelerators in the LHC is displayed in Fig.8. The ATLAS experiment at the LHC consists of many components. Each of these components meets some of the technical requirements of the main projects. In general, these requirements are tracking, detecting, measuring, identifying and finally saving the details of information of all the interesting produced particles for later studies. Fig.9 represents a quick view of the different parts of the ATLAS detector.

## 4.1 *Inner Detector (ID)*

The inner detector is made of three parts, the *Pixel Detector*, the *Silicon Tracker (SCT)* and the *Transition Radiation Tracker (TRT)*. They are the

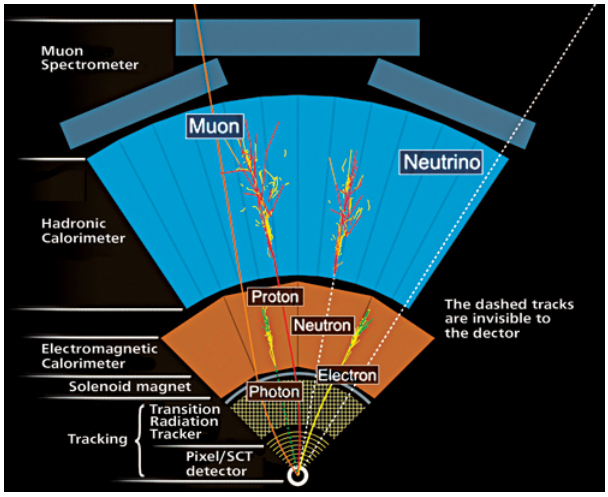


Figur 9: The transverse slice of ATLAS detectors at CERN.[19]

closest components of the ATLAS detectors to the interaction point (IP) region. They are shown in the Fig.10.

**Trackers:** Tracking is the process that is used to find out the particle path. A part of identifying the particles is done in trackers. It consists of several thousand electronic modules to detect charged particles. Since these detectors are the first components in the ATLAS detectors system that receive the particle signals in the collision, the precision and granularity should be as high as possible. The first detector, the pixel detector ,is the nearest part to the IP region. It is made of three barrels with different radii that is covered completely with millions of silicon pixel elements. In addition to having high granularity, it is also a correspondent device for finding the short lifetime particles. It provides very high resolution and measures the impact-parameters[1] in the found interactions.

**SCT:** The SCT is the second tracker and is made of four barrel layers. They cover the pixel detector barrels and the beam line location. It operates similar to the pixel detectors. The electronic modules are covered by a very thin layer of silicon. When a charged particle passes the silicon water of the

[1]The perpendicular distance between the target particle and the initial line of motion of the collided particles.

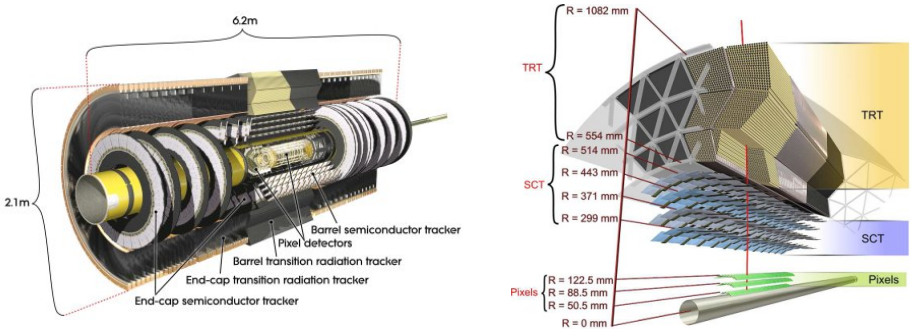


(a) (b)

Figur 10: The inner Detectors. a) A quick view of the inner detector. b) The Drawing shows the sensors and structural elements, the track successively the berylium beam-pipe, the three cylinderical silicon-pixel layers, the four cylindrical double layers of barrel silicon-microstrip sensors (SCT) and the barrel transition-radiation tracker (TRT) modules.[20]

SCT module creates the electron-hole pairs. In the SCT holes are collected by the stripes and make very small electric current. By tracking this electric current it is possible to recognize the movement and position of the charged particles.

**TRT:** The TRT is the last part of the inner detector and is located at the out side of the silicon detector. There are a large numbers of tubes that are filled by a mixture of 70% Xe, 27% $CO_2$ and 3% $O_2$ gases[20]. When the charged particles pass through these tubes, they ionize the gas and can release photons and electrons. The photons from transition radiation are collected later with the Xe component of the gas and free electrons. There is also a 31$\mu$m gold-plated tungsten anode wire[20] in the middle of the tubes that collects electrons or negative charged particles. It can also detect very weak electric currents. The amount of negative collected particles by the golden wire is varied for different type of particles. Hence, this method helps the ATLAS detector to distinguish the nature of the initial interacted particles with the gas and help identifying the particles.

## 4.2 *Calorimeters*

The knowledge about the charge and momentum of a particle is one step forward to identify a particle in the ATLAS experiments but to complete the

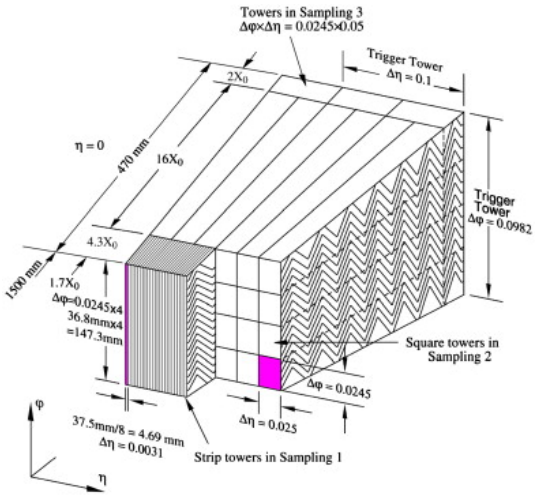


Figur 11: The LHC electromagnetic calorimeters. The Sketch of a LAr EM barrel module where the different layers are clearly visible The granularity in $|\eta|$ and $\phi$ of the cells of each of the three samplings is also shown[21]

identification of a particle, the energy of the particles should be measured. The moving particle should be collected completely to make the measurement of the energy possible. This is achievable by the calorimeters in the ATLAS detectors. The calorimeters are the middle parts of the detector. They are advantageous for the stable particles which pass the pixel and the SCT detectors but not for short lifetime particles. There are two types of calorimeters: Electromagnetic and Hadronic calorimeters.

### 4.2.1 *Electromagnetic Calorimeter (EM)*

The EM calorimeters can measure the energy of the charged particles and also neutral particles, primarily electrons and photons. They are made of many compressed thin layers of lead and stainless steel. There is another component, called *particle collector* which are liquid Argon based. Argon has linear behavior and has high stability in the time and has the radiation tolerance[31]. These collectors are located between each of the compressed layers. There are also many copper electrodes for collecting the negative charges behind this argon layer. This system covers the area with the pseudorapidity between $1.4 < |\eta| < 3.2$. When a charged particle meets the collector, it

interacts with the material and produces low energy particles like electrons, positrons, and photons. Hence, before the initial particle passes the layers of the calorimeter and stops, it produces a large shower of new particles. This low energy particle shower passes the liquid argon and ionizes the atoms and creates more negative charge electrons and positive charge ions. The negative charge electrons are attracted by copper electrodes where it can be converted to electric signals and finally the energy of the original particle is measured.

### 4.2.2 *Hadronic Calorimeter*

The Hadronic calorimeter is the large calorimeter located outside of the EM calorimeters. Those particles which have a longer lifetime and make strong interactions, pass through the EM calorimeter; like protons, pions, kaons and in general, quark-based particles like hadrons enter the hadronic calorimeter. The material of the calorimeter is steel and there are many scintillator sheets called *tile*. The scintillator sheets material radiates light when they are exposed to charged particles. These light pulses are transmitted to the photomultipliers tubes by the optical fibers which cover the region of $|\eta|$ <4.9. The produced pulses later can be measured and converted to the electric signals. The signals show the amount of energy each shower of particle carries and since this shower of energy is equal to the energy of the initial particle, with a calibration constant, it presents the energy of the parent particle.

## 4.3 *Muon Spectrometer*

The last and the largest part of the ATLAS detector, is the muon spectrometer. Muons are very massive particles in comparison to electrons. With a long lifetime about $2\mu$s. None of the inner detectors can stop muons. Therefore, they pass all the other layers and just leave tracks. Thus, there should be another detection technique to measure the energy and momentum of the muons. The muon spectrometer has been designed to cover almost all regions with $|\eta|$ <2.7 such that the muon might travel and pass through to the point where it is stopped or at least is measured by the muon spectrometer. As it is shown in Fig.12 four different chamber technologies are applied on the muon chamber. For covering the complete momentum resolution, the position of these stations are important. These chambers are installed in two directions: horizontally and vertically, to catch the muons in both possible dimensions. The three cylinders are rounded the beam axis in the muon chamber with

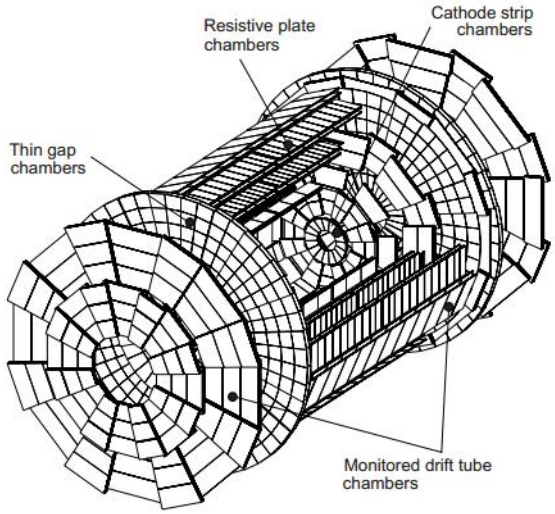


Figur 12: Three dimensional view of the muon spectrometer instrumentation indicating the areas covered by the four different chamber technologies.[22]

barrel radii of 5, 7.5 and 10m[22]. These radii has chosen to coverage the whole pseudorapidity range of $|\eta|$ <1. The rest part of the pseudorapidity range, 1< $|\eta|$ <2.7 are covered by the end-cap chambers which are four disks at distance of 7, 10, 14, and 21-23m[22] from the interaction point. The strategy of the muon spectrometer to measure the muon is deflecting the muon track by the high magnetic force that is produced by the superconducting air-core toroid magnets[22]. The process of tracking near the interaction point where $\eta$ is larger, is done by the *Cathode Strip Chambers (CSCs)* and for lower values of $\eta$, it is determined by the *Monitored Drift Tubes (MDTs)*. The triggers of the Muon spectrometer detect and record the data of the muons by the *Resistive Plate Chamber (RPC)* which covers the region of $|\eta|$ <1.05 and for the region of 1.05< $|\eta|$ <2.4 by the *Thin Gap Chambers (TGC)*.

Fig.13 shows that a small segment of this chamber consists of many tubes filled with gas, when the muon passes through these tubes it interacts with the gas and leaves many charged ions and electrons which are collected by the wire at the center of the tube. Measuring the time which takes for the charged particles to drift from the starting points, makes it possible to determine the position of each muon when it is passing through the muon chamber.

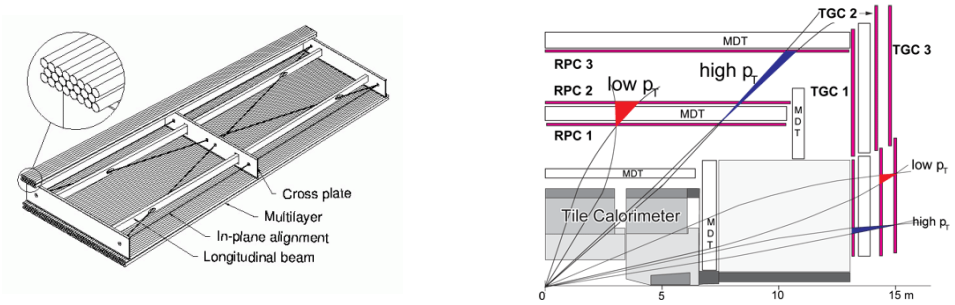


(a) (b)

Figur 13: Muon Spectrometer. a) A schematic view of the monitored drift tubes. b)A schematic view of the muon system. The positions of the trigger chambers are highlighted in red with tracks indicating the low $P_t$ and high $P_t$ trigger coincidences[23].

## 4.4 Triggers

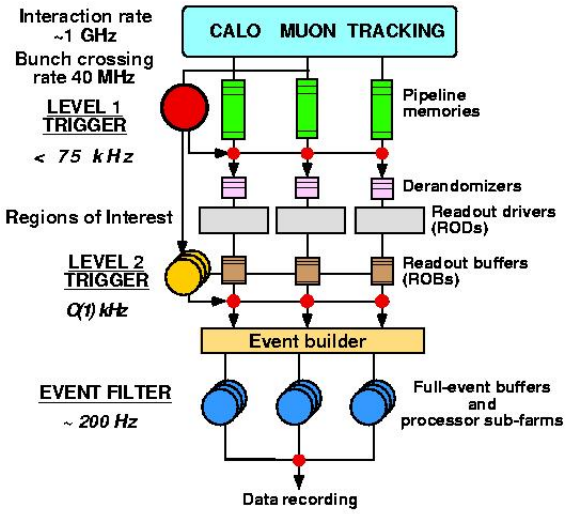


Figur 14: A simple view of LVL1, LVL2 and EF triggers.[25]

After detecting particles by the detectors, the signals should be stored somewhere to be investigated later. Particles interact with the detectors with very high rates (GHz) and the number of these interactions are much more than the capacity of all the ATLAS storage systems. Thus, many of these signals cannot be kept and are terminated. In this circumstance, a trigger is

the solution to this problem. When just a small fraction of the particle information is stored, the trigger does a quick selection between passing signals and recording ones which are more interesting. These records will be used later in *the object identification* process to reconstruct the event. The trigger process is implemented by dividing the trigger into two main levels. *First Level trigger* and *High-Level Trigger (HLT)*. Fig.14 represents the output of each level trigger and the data from additional detectors are the input to the next trigger. Through each level, the process reduces the signal rates and gives the system more time to make a better decision and record the best events.

- **First-Level Trigger (LVL1):** is a hardware based trigger and the first data recorder that collects the signals from the produced particles after being detected by the detectors. It makes the decision just from the information from calorimeters and muon detectors. The *calorimeter triggers* consists of an electron, photon, tau, hadron and jet triggers. There are about 7200 relatively coarse-granularity trigger towers in the calorimeters[24]. All these triggers have many processors which identify particles in the determined local regions of $|\eta|$ <2.5. These local regions are defined with different core sizes for varied particles and determine the isolation criteria for each type of particles. Moreover, the information in the *muon trigger* is provided by *Thin Gap Chamber (TGC)* in the endcap and *Resistive Plate Chamber (RPC)* in the barrel. The algorithm for recording the high-$P_t$ and low-$P_t$ muon thresholds is based on the number of hits in the inner layers and outer layers. The prepared data is forwarded to the *Central Trigger Processor (CTP)* and *Region Of Interest Builder (RoIB)*.
  The first level triggers have to make the fastest decisions in about 2.5$\mu$s[24] for selecting the interesting signals through thousands and thousands of signals per second. This time is spent for transferring the signal from the detector to the trigger electronics while the rates of the signals when interacting with the detectors, is up to 40MHz. It should be considered that the time duration between two bunch-crossing is at least 25ns. This time scale is much shorter than the ability of a trigger to take a right selection. Hence, the information of detectors before being selected by the LVL1, is saved in pipeline memories. This stored information will later be sent to the *Read Out Drives (ROD)* after being

selected by LVL1. In ROD the first calibration is done over data and they will be sent to the *Read Out Buffers (ROB)* for later processing in high-level triggers.

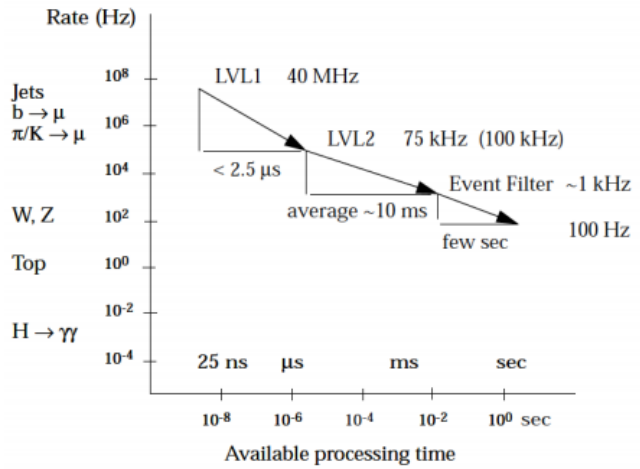


Figur 15: The three levels of the ATLAS triggers and their event rates and processing times.[22]

- **High-Level Trigger (HLT):** is software-based triggers. It involves *Second-Level Trigger (LVL2)* and an *Event-Filter Trigger (EF)*. The input of HLT trigger can be shared simply between LVL2 and EF triggers. This trigger checks the regions of interest(ROIs) of the LVL1 but in more detail and at full granularity. There are series of steps which is called a *trigger chain*. The trigger chain steps need to be confirmed by a kind of signature before forwarding each process to the next level. The HLT trigger has the potential to reject any process that does not have this signature. It helps the system prevent delay and choose more interesting signals. The HLT triggers also imply the *feature extraction*. They identify the data coming from RoI. Identification is specifying if the coming data is a track or a calorimeter cluster. The HLT algorithms after checking the data with the identification criteria, forward it to the LVL2 triggers. The data passing the LVL2 trigger later is transferred to EF trigger after reducing the rate up to about 3.5kHz[20]. Moreover, in the EF trigger some calibrations are applied on features, e.g: Bremsstrahlung recovery for electrons and conversion recovery for pho-

tons. The EF trigger then increases the rate of the data to 200Hz[22]. This rate allows the data to be used for offline analysis.

# 5 The Object Identification

In all particle physics experiments analyses, reconstruction and identification of the object play a critical role in the process of analyzing and obtaining accurate results. This chapter covers the definition and identification of the objects which are participated in the top quark pair and also explains the *Event selection* process which is used in this study.

The first step of identifying an event is the *object definition*. In this step, particles are distinguished in an event. It is a method of finding a particle in an event by gathering the related categorized information of an object and reconstructing the produced particles of the event. This process helps in tracing back the particles and reach to the event primary vertices (collision point) and the source particles. This chapter deals with identifying different types of the objects that are produced in the $t\bar{t}$ decay. These objects are electrons, muons, jets and missing transverse energy.

## 5.1 *Electrons*

Electrons as one of the final-state leptons in the top quark pair events are reconstructed by the EM calorimeter. They may be reconstructed either by a standard cluster-based or a track-based algorithm. Since they are charged particles, they can be traced by the trackers in the inner layers of the detector. In almost all of the interesting analyses there is at least one or two electrons that come from a misidentified hadrons, non-isolated electrons from heavy-flavour decays, jets and electrons from photon conversions. The original electrons according to the top quark dileptonic decay, are produced by W-boson decay ($W \rightarrow e\nu_e$). The electrons which are produced from the other sources like Z-boson are considered as background electrons in this analysis. Here is the list of important cuts that are used for finding the isolated electrons[26].

- **Author:** The electrons should be chosen from the right author. The author is the algorithm used to create electron candidates. In this study the electron author might be -1- which means the electron is standard and is not track-based or should be -3- which means the electron is found from both standard and track-based algorithms.

- **ID criteria:** This is the criteria of the inner detector,$|\eta_{cl}|$ <2.47, where $|\eta_{cl}|$ is the pseudorapidity of the electromagnetic cluster associated with the electrons[26]. Outside of this region is the out of inner detector. There is also an excluded transition region of 1.37< $|\eta_{cl}|$ <1.52. The electrons of the excluded region are assumed to carry a low energy as they move a region between barrel and end-cap. Hence, they are rejected.

- **Tight++:** The electrons are tested for being *tight*, *medium* or *loose*. This cut represents how much the criteria is tight for being detected in a straight line to the detector. The TRT electron identification is applied to reject the charged hadrons by limiting the number of hits in TRT. Tight cuts are also very effective in identifying electrons by rejecting jets up to about 50000 rejections[27].

- **Transverse energy of electron:** The leptons from top quark decay are expected to have high transverse energy. This variable should be $E_t$ >25 GeV.

- **Isolation cut:** There is a specific criteria for each particle in the event that makes it isolated and safe from being overlapped by the other objects. The electron isolation criteria in $t\bar{t}$ decay is defined by $EtCone20@90$ and $PtCone30@90$[26]. The calculation is applied by the *EisoTool* program on the data.

- **Electron/jet overlap removal:** The another part of the electron isolation cut is checking the electron and jet overlap criteria. Particles of the jets in top quark pair decay usually travel through a conical area after being created. The isolation criteria of each particle is also considered as a cone shaped area from the produced point. The particle is isolated if this is not occupied by any other particle. The overlapping cut is based on the difference between the angular properties of the particle and the jet. This difference is calculated by $\Delta R = \sqrt{(\Delta\phi)^2 + (\Delta\eta)^2}$ and is considered in two forms in this study:

  - **Overlapped-jet removing:** If an electron and jet overlap within an angular region of $dR(e, jet)$ <0.2, then the jet is really an electron, and it should be removed from the event[28]. This cut is for removing jets which are overlapped with electrons.
  - **Overlapped-electron removing:** After removing the jets that are overlapped the electrons from the event, the electrons are checked. They should not be close or inside of the remaining jets. The electron will be rejected if $dR(e, jet)$ <0.4. This value is larger than the first cut, due to the larger area that a jet occupies. The involved jets should have $P_t$ >20 GeV.

.

## 5.2 *Muon*

Muons are stable particles. Due to the relative massive size of the muon it carries a remarkable part of the energy of the event. In $t\bar{t}$ (e,$\mu$) dileptonic decay, muons as well as electrons are produced by W-boson decay but there are other particles like *Pion*, *Kaon* and also Tau lepton($\tau$) which can produce muons. The muons are produced by the latter sources are considered as background in this analysis.
In top quark pair (e,$\mu$) dilepton decay, a muon is first recognized by its track.

High-quality muon tracks, create the minimum number of hits in the tracking detectors as they carry high energy and do not generate noise in the detectors. Reconstruction of muons in this selection is done by the *STACO* software. STACO is an identification software package that helps the track to get its form. It is used to combine the reconstructed tracks which are produced in the inner detector and those are formed in the muon spectrometer and finally identify muons at their production vertex[33]. The overview of the muon cuts in the $t\bar{t}$ decay are listed here[26]:

- **Tight:** The selected muon for $t\bar{t}$ decay event should be a tight muon which determines the efficiency of the detector to observe the object. The tight cut provides the high possibility to catch good muons and reject the backgrounds.
- **ID criteria:** The coverage value of $\eta$ in the inner detectors for muons is $|\eta| < 2.5$.
- **Transverse momentum:** Each of the muons should have the $P_t > 20GeV$.
- **Isolation cut:** Muons isolation criteria is $EtCone20 < 4GeV$ and $EtCone30 < 2.5GeV$.
- **muon/jet overlap removal:** After removing all the overlapped electrons and jets, there should be no overlapped muon with the remained jets in the event. Muons are rejected if $dR(mu, jet) < 0.4$. The included jets should have $P_t > 25GeV$ and $|JVF| > 0.75$.

## 5.3 *Jets*

Jets are formed by the long-lived hadrons which remain after the hadronization. Their directions are usually the same as the original quarks or gluons in the hadronization. In principle, they can represent underlying events and showers of charged and neutral particles in the EM and hadronic calorimeters. They are also a good source to study the original quarks as it is supposed that a part of the properties of the original quarks are transferred to jets.

In this QCD multi-jet events with at least two jets, only jets in the tail of the detector response can be misidentified as leptons. Thus, jets are one of the

sources of producing the non-original leptons or *Fake leptons*. In a hadronic collision, like a proton-proton collision, and in the top quark pair event, a jet clustering algorithm is the main tool in distinguishing the events. Basically jets are recognized by the algorithm they are reconstructed with. Algorithms are the tools for contrasting the properties of boundaries of jets[26].
Jets in the top pair decay are clustered with the infrared and collinear safe anti-kt algorithm[8]. This algorithm focuses on the transverse momentum of the particles, $k_t$, as the important parameter. It recognizes the soft and hard particles and based on the momentum determines the distance between soft and hard particles in different conditions in the jets. These analyses shows, this distance is larger between the separated soft particles than hard ones. It implies that soft particles create cluster with themselves not as fast as hard particles with each other. For example, when there is a hard isolated particle with no hard neighbors in a distance about 2R (R is a circle of radius around the particle), the soft particles within the distance R around the hard particle can simply be stacked up by the hard particle and form a conical jet. The result of the anti-k$_t$ algorithm indicates that the hard particles modify the shape of the jets when the boundary of the jets are specified mostly by soft particles[26].
The jet energy deposition is in the electromagnetic energy scale and due to the imperfect detector response, this energy should be calibrated to obtain the real value of the energy in jets. In this process the jet energy scale(JES) as the factor of correction, is applied on the jet energy deposited by the calorimeter and yields the original energy of the jet parton. In this analysis all the jets are from AntiKtTopoEMJets (EM+JES callibration). The important cuts over the considered jets are[26]:

- There are at least two jets in each event.
- The conical area of each jet shows the boundary of a jet. The cone size in clustering algorithm is dR = 0.4.
- The transverse momentum P$_t$ of the jet is at least 25 GeV and the pseudorapidity of jet is $|\eta_{jet}| <2.5$.
- The jet vertex fraction is $|JVF| >0.75$ to reduce the pile-up effects. JVF is a method to find out the jets that are produced in the hard scattering processes. It tracks the particles in jets and recognizes their

right primary vertices to measure the probability of a jet to be produced from a specific vertex. This kind of jet selection is less sensitive to the contributions from soft collisions through the pile-up process.

### 5.3.1 *Identifying Jets By b-Quarks*

The b-quark is one of the important quarks in the top pair decay analysis as the possibility of finding top quarks in the events with at least one jet originating from b-quark or its anti-quark is high. The light flavor jets which are considered background in this analysis are usually produced by W-boson decay and have a very small fraction of b-quark jets. The b-quark has a large enough mean lifetime of order of $10^{-12}$s[30] to reach to detectors but through this travel lots of other particles, such as up and down quarks and gluons, surround the b-quark and make a hadron.

There are other created hadrons by the collision that accompany the b-quark in this event but the specific hadron which is considered in this study is B-hadron. A bit further, in the scale of picometer, from the primary vertex, the B-hadron decays into many lighter hadrons which none of them contains a b-quark. This decay creates the secondary vertex. By zooming out from this small scale, the short travel of the B-hadron and the secondary vertex is disappeared. Thus the only option to identify the jets which are produced by B-hadrons is tracing back the jet partons in the trackers and find the secondary vertex. The jets which are coming from secondary vertex are called b-tagged jets. In b-tagged included events, b-quarks can be misidentified by c-quarks since c-quark can produce jets and they have almost same mean lifetime as b-quark. Hence, the c-quark has this potential to be the fake b-quark in the $t\bar{t}$ decay.

There are different algorithm for recognizing b-tagged jets. The MV1 is a neutral network-based algorithm that gets its output weight from the combination of other algorithms such as[34]:

- The (JetFitterCombNN) algorithm to find the c-quark and b-quark decay position in the jet.
- Impact parameter-based algorithm (IP3D + SV1) to find b-jets and light jets in MC simulation .

- Secondary Vertex-based algorithm (SV0) for finding two-track vertices.

In this analysis, at least one of the jets should be b-tagged and for this approach 70% of the b-tagging efficiency is considered.

- MV1 for 70% ($weight > 0.601713$)

### 5.3.2 *Bad Jets*

The other issue that must taken into account in finding the good jets in events with large number of jets, is recognizing the *Bad Jets*. Fake jets which are coming from the particles and the interaction with the calorimeters materials, electric noises in the detectors, cosmic ray showers and the beam background could produce bad-jets. *Jet cleaning* is the method of removing bad jets from the events. The offline loose cuts of this method are listed here.

- **HEC spikes:** The first variable of the cut is referred to HEC fraction. This fraction is measurable in the Hadronic End Cap calorimeter and is the fraction of energy in the reconstructed jets. HECQ is a fraction of cells in the calorimeter that is measured by end cap region. It yields its value when the interaction of particles and calorimeter cells make the electrical signal. when the Q value is very close to one, the signals from the calorimeter cells are calorimeter noise[31] and should be removed. The HEC value criteria is $HECf >0.5$ and $|HECQ| > 0.5$.

- **EM coherent noise:** The energy of reconstructed jet in the electromagnetic calorimeter is measured by the EMf fraction, when EMf is equal to one, it means all of the energy of the jet is deposited in the EM calorimeter. LArQ is as same as HECQ, the only difference is that the LArQ is measured in the electromagnetic calorimeter[31]. $EMf >0.95$ and $|LArQ| >0.8$ and $|\eta| <2.8$.

- **Non-collision signals (cosmics):** Except the signals come from the backgrounds, fake particles, and the noise from the detectors, there are the other signals do not originate from the hard collisions. For instance, both muons and tauons can be observed by the detectors when the cosmic rays interact with the atmosphere. The Neutrinos can also be produced by the atmospheric interactions. For preventing the analysis to consider the cosmic rays, the absolute flight time between the collision and hits to the hadronic calorimeter have to be less than 25ns in this study[31].

## 5.4 *Missing Transverse Energy (MET)*

The total energy in the top quark pair event before and after the decay is conserved. Therefore the summation of energy of the top quark pair is equal to the summation of the whole of the energy of the later particles which are produced in the top and anti-top decays. In addition to all the obtained particles which are observable, there are neutrinos which are only weakly interacting and are not detectable by the ATLAS detectors. Hence, they only hint their existence by the energy they take in the event. Beside the energy from neutrinos, there are always another sources of missing energy that are due to the different reasons, like interactions between the particles and detector materials, neutrinos from semi-leptonic decays, non-linearity of the calorimeter response ,minimum energy thresholds and inefficient detector regions[8]. All the energy yielded by these sources can be misidentified with the energy of the neutrinos in the analysis. If the latter energies that are coming from sources non-related to neutrinos, are ignored, *Missing Transverse Energy* can be defined by:

$$\sum_{reconstructed particles} \vec{P}_t + \vec{P}_t^{miss} = 0 \tag{11}$$

$$\vec{P}_t^{miss} = - \sum_{reconstructed particles} \vec{P}_t \tag{12}$$

It is almost never possible to subtract all sources of missing energies from reconstructed particles in an experiment, hence the missing transverse energy is almost always mixed with the fake missing energies. Most of the cleaning methods in the list of cut flows are there to prevent the not related energies to become misidentified by missing transverse energy. In general for finding $t\bar{t}$ (e,$\mu$) dileptonic channel decay, the MET variable is selected from $RefFinal\_MET$ or refined calibration MET. This is a calibration method that is applied for both Monte Carlo samples and data in this analysis.

## 5.5 *Event Selection And Reconstruction*

The event selection clarifies the criteria of the analysis and gives the possibility to reconstruct the objects in the event based on the purpose. The purpose of event selection in the $t\bar{t}$ decay charge asymmetry analysis, is to maximize the ratio of the signal contribution from dilepton (e,$\mu$) channel to the background. For finding and selecting the top quark pair event all the

selected and identified objects which belongs to this event should come into account. The objects which participate in the $t\bar{t}$ event selection reconstruction is one electron, one muon, at least two jets, and missing energy which refers to two undetected lepton-neutrinos. The Event selection is applied on both MC samples and raw data. There are some selections that are just applied on MC samples and not on data, the criteria of all these selections for the $t\bar{t}$ decay is listed here. These cuts are also similar to the selection cuts of the official ATLAS publications of the year 2011[32].

- **True dileptonic event:** This cut is applied just to the MC samples. In the true dilepton cut, both leptons should be true leptons and it is tested by checking the parent-ID of the detected electron and muon in the event. When the background is under investigation, the parent-ID should refer to W-boson and Tau lepton.

- **Trigger region:** When a lepton passes a trigger,it is said it has *fired* the trigger. The trigger is proved by checking some determined items for each region. These items for electrons based on the region and the run number can be one of $EF\_e20\_medium$, $EF\_e22\_medium$ for MC samples and $EF\_e22vh\_medium1$, or $EF\_e45\_medium1$ for Data. In muons they are $EF\_mu18$ for MC samples and $EF\_mu18\_medium$ for Data. At least one of the electron or muon should pass the region till the event gets accepted for this selection.

- **Good vertex:** The primary vertex, in fact, is the point that the event is originated from. Having selection on primary vertex is useful since it helps to reject not interesting particles such as particles from backgrounds and also cosmic rays. The $t\bar{t}$ decay event should have at least 5 tracks in the primary vertex to pass the good vertex cut.

- **At least two isolated leptons:** The event should have at least one isolated electron with $P_t$ >25GeV and one isolated muon with $P_t$ >20GeV. The leptons of this event should pass the object selection criteria for electron and muon to be isolated.

- **e/mu overlap:** Since the electron and muon in the event are isolated, there should be no signs of overlapping between them. The overlapping criteria is defined by $\Delta R = \sqrt{(\Delta\eta)^2 + (\Delta\phi)^2}$ where $\Delta\eta$ is the difference between the pseudorapidities of the electron and muon and $\Delta\phi$ is the

difference between the azimuthal angles. This value should not be less than 0.2, otherwise they will be considered as overlapped leptons and should be removed from the event.

- **Ht cut:** Based on the type of analysis ,the summation of the momenta of all the components or just some of the components of an event is called the Ht Value. In this analysis, the Ht value is summation of the momenta of the selected electron and muon with the highest $P_t$ and the two jets from selected jets with the highest momentums. The Ht cut for top pair dilepton (e,$\mu$) decay should be larger than 130GeV per event.

- **Exactly two leptons:** In the $t\bar{t}$ (e,$\mu$) dilepton decay analysis, there should be exactly one isolated electron and one isolated muon in each event. Hence if there are any more isolated leptons from both types, the one with the highest momentum should be selected. So that the number of electrons and muons should reach to exactly one after passing this cut.

- **Trigger matching:** Through all the leptons that are checked in the trigger region, there should be at least one lepton (one electron or one muon) that is matched with the fired objects in the trigger. This value is checked by calculating the $\Delta R$ between the trigger object and the lepton tracks. The value should not be larger than 0.15. This cut is applied to both electron and muon.

- **Opposite sign leptons:** In this study, the two leptons (e,$\mu$) need to have opposite charge.

- **Truth matching:** This part of the analysis is done only for MC samples and is applied on both selected electron and muon. In this cut some properties of the leptons like, the type of the lepton, original type, and the background type are checked. Each of the particles have a code number for these variables in MC sample. If all of the code numbers are matched with the expected defined code numbers for the $t\bar{t}$ event final leptons, it is said that the particle is matched. This test helps to find the right lepton in the simulation. For being selected as the final lepton, both electron and muon should pass this cut successfully.

- **LArError Check:** The value of LArError variable is obtained by LAr calorimeter. It discriminate the noise bursts and data integrity errors. The filtered values of this cut for release (17) are the signals with $LArError > 1$.

- **B-tagging:** It was explained before that B-tagging is one of the methods to distinguish jets which are producing by b-quarks from the other type of jets. In this study, at least one of the selected jets in the event should be B-tagged.

# 6 Analysis Techniques

This chapter is the last part of this study it deals with methods of analyzing and the final results of the charge asymmetry in the $t\bar{t}$ dileptonic decay in (e,$\mu$) channel.

## 6.1 Analysis Computing Requirements

All the raw data and information from the ATLAS detectors are filtered in the triggers. Although this raw information forms the main part of the later analysis, not all of it is used directly in the calculations. The raw information needs categorization and preparation to make it more accessible. Hence many collaborations and analysis tools has been created to support the requirements. Some examples of these softwares are explained here briefly.

- **The Athena framework[35]** is designed as a component-based architecture. In this framework a large number of data can be separated, shared and reused easily everywhere by analyzers. Data is accessible in two forms of online and offline and the compilation language is C/C++. It also uses the Python language to execute code over dataset files.
- **Root[36]** is the other framework which has special storage methods to save data as a set of objects with their properties. These objects have NTuple/histogram format and various types and provide the possibility of direct access to each required object separately.

- **The LHC Computing Grid (LCG)[37]** is a worldwide distributed analysis network for the large scale analysis that cannot be done in one server. It spreads out data between several servers in different places. By this method several analysis can proceed at the same time.

## 6.2 *The Simulation Procedure*

In a quick view, the simulation procedure consists of several steps shown in Fig.16.

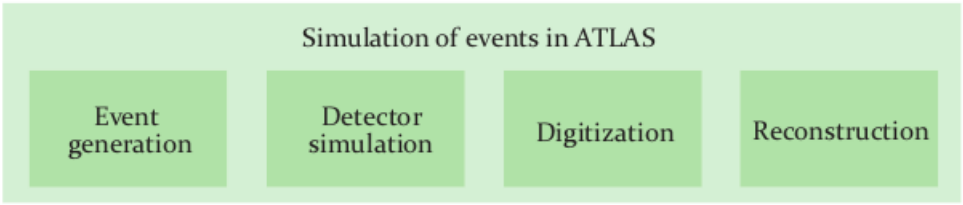


Figur 16: Consecutive steps in the simulation of collision events.

### 6.2.1 *Event Generation*

There are a lot of Monte-Carlo samples to provide the information of the event-generation. The basis of Monte-Carlo is the use of the random numbers and probability statistics.The information of MC samples is produced by the *General-Purpose Monte-Carlo (GPMC)* generators[38]. GPMC generators are used to estimate the signals and backgrounds in the high-energy processes. They cover different scales from very short distances about QCD scales up to very large scales like hadron formation scales. Fig.17 presents the different processes of the event-generation step in simulation of events in the ATLAS experiment.

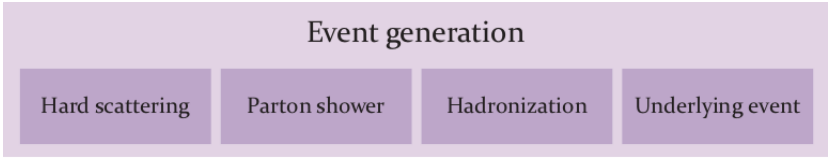


Figur 17: Processes of the event generation.

A random configuration of the possible candidate events in parton interaction through hard scattering, are obtained in event generation process. All the partons kinematic properties like the momentum and weight of these partons can be calculated by, in this process. All the simulated partons in the event generation process will be the subject of parton showering and decay. The parton showering creates a bunch of particles and gluons and this step of event generation is simulated by the parton shower models. Since the hadronization is not in the scale of perturbative QCD, this step should be modeled by the fragmentation models which one of the practical one is *Lund String fragmentation*. The last step is *Underlying events* that will be explained in the Pileup section with more details.

### 6.2.2 *Detector Simulation*

*Detector Simulation* helps in recognizing the position of the particles in the detectors and the deposited energy in the different components of detectors. In general it is clear how the particles interact with the detectors. This process is done by a simulation program which is called GEANT[39]. By identifying and tracking back the elementary particles in the matter in an experimental setup, GEANT can describe the geometric state of the particles in the detectors in addition with the modeling of different interactions of the particles with the ATLAS detectors material.

### 6.2.3 *Digitalization*

The interaction between the detector and the particles are modeled in the *digitization* step. The hit particle deposited energy obtained by the detector is converted to the electronic signals. By digitization process the energy of all the particles which make signal or any interaction hit with the detector materials are calculated and the model of movement of these particles in the detector are simulated as similar as when the ATLAS detector records the data information.

### 6.2.4 *Reconstruction*

This simulated events is now in the form of a series of raw events which is identical to data. Hence, the required reconstruction on data and simulation starts in the *reconstruction* step. A number of different algorithms are applied on both simulated and data events. The process unpacks the events from

each detector separately and interprets and calibrates for each detector. The output of the reconstruction step creates a large number of the physics objects for the analysis. It also produces the other requirements of a good event like vertices and tracks.

## 6.3 *Data Quality*

Physics analysis requires well defined data taken under stable conditions. The Data Quality(DQ)[40] information helps in defining a good dataset. It gathers this information by DQ flags which are indicators of the data quality. The mechanism of the DQ flags, reflects the overall data quality status of the ATLAS (sub-)detectors. DQ flags behave like the traffic light and the feedback of this control is in form of different colors for different status per luminosity block.

When the data quality information is discussed, two concepts of list of physics runs and *Luminosity Blocks* are introduced in the form of *GoodRunLists (GRLs)*. The luminosity-block here refers to the time duration for taking the data and the data-quality criteria is the item that forms the goodrunlists to select the good data for the analysis. DQ information criteria are formed by the detector and other combined performance DQ flags[41]. By applying these criteria on the list of all valid physics runs and luminosity-blocks, a good run lists is configured.

The monitoring system of data taken from triggers is divided into two parts of online and offline based on the quality of the data. By online data-monitoring, a user has more access to the original data from detectors. There is no reconstruction of this data. Although the quantity and distribution of this data is not the best, but they are good for getting quick responses from the detectors. In offline mode of the data-monitoring, the recorded data is coming from all the detectors and the data reconstruction is applied separately for each sub-detectors. It also gives this possibility for having both automatic and manual monitoring. The data is used for this study is from the second mode, the offline data quality monitoring.

## 6.4 *Luminosity*

The luminosity is an important variable that should be taken into account when a lot of particles with different cross-sections in the event are involved. Basically luminosity is the interaction rate of the number of particles in the bunch crossing in the collision. The interesting issue about the luminosity is that it can have the same result even if it is calculated over different collisions. The formula below confirms this fact:

$$\frac{R_X}{dt} = \sigma_X . L \tag{13}$$

in this formula $\frac{R_X}{dt}$ is the rate of the collision x and depends on the number of collisions per second. $\sigma_X$ is the cross-section of the two colliding beams. It is the area of the particles in the first beam that the particles of the target beam collide with and make the event happens. This area is also independent of the type of the collision and the particles in the event. The last variable, $L$, is the luminosity of the process. The formula which the fixed-target luminosity is calculated with directly is:

$$L = \frac{N.\rho_t.l}{s} \tag{14}$$

here $\frac{N}{s}$ is the number of particles per bunch crossing per second, $\rho$ is the density of the target beam, $l$ represents the length of the collision. The target beams are moving beams, in the ATLAS experiments. Obtaining the accurate value of collider luminosity (per bunch crossing) is more complicated than what is explained here. The density depends on the position and time, $\rho(x, y, s, s_0)$ and all these changing variables should be taken into account in the calculation. The obtained integrated luminosity of the proton-proton beam collision data, used for this study after selecting the corresponding GoodRunList is:

$$\int L.dt = 4.58 fb^{-1} \tag{15}$$

The integrated luminosity in the MC samples are different from the calculated one in the data. Thus all the histograms and results are multiplied by the scale factor or the normalized value at the end, to make a complete comparable simulation model for analyzing.

## 6.5 *Pile-Up*

In a high energy process the partons which have too low momentum to participate in hard collisions, participate in lower energy interactions in the background. These interactions make *underlying events*. Although the probability of creating multi-hard scattering events is low ,there is an option that can increase the number of these interactions in the bunch. It arise when there is an *in-time pile-up* contribution. Pile-up, in general, occurs when the readout of a particle detector includes information from more than one primary beam particle interaction. These multiple interactions that might come also from underlying events are called piling-up". In in-time pile-up due to the instantaneous luminosity, there is a multitude of soft interactions from other proton-proton collisions in the same bunch crossing which increase the contributions to the final events. If this process does not happen and there are not many soft interactions in one bunch crossing, the other particles from the final state of the other bunch crossings create *out of time pile-up* contribution in the event. However, due to the very low momentum of the final particles of underlying and pile-up events, there are some difficulties in describing these kinds of events by perturbative QCD. For modeling the data correctly, almost all of the mentioned processes should be considered for simulating signal and background processes.

### 6.5.1 *Pile-up Reweighting*

Pile-up reweighting is a technique to match the pile-up conditions of the MC samples to the data. The condition of pile-up in the data is changing over time while, pile-up in MC samples is a fixed number of interactions per bunch crossing of the main parton and also consists of occurred in-time and out-time pile-up contributions at the bunch crossing. This mismatching can make a problem in making the simulation for the further comparisons of MC samples and data pile-up models. Thus, pile-up reweighting corrects the event weight in MC samples and matches it with the measured one on the data. Pile-up reweighting is just for MC samples and is applied before starting any analysis on the samples.

## 6.6 *The top Quark Pair Modeling*

Modeling the top pair decay requires some preparations on the signal, data and the background which are applied by the event selection cuts to all of them. Later the needed corrections and normalizations are applied to signal and background in order to be able to compare them to data. The results depend on the definition of signal and the background events.

### 6.6.1 *Signal Leptons*

In all the final leptons that are produced in the $t\bar{t}$ decay, those leptons which are produced by W-boson decay in the hard-scattering events are the *Signal leptons*. The signal leptons in this study are electrons and muons in $e\mu$ channel of the final state. The $t\bar{t}$ simulated MC signals are obtained from the next-to-leading order, *T1-MC* samples and it is specified by *no full hadron* which means at least one of the W-bosons from top and anti-top quark decay, does not decay to hadrons directly. The momentum energy of the ATLAS for this experiment is 7TeV and it is chosen from the last generation of databases mc11c at the end of the year 2011. The samples are from NTUP_SMWZ data-type and is modeled by the Standard Model. The parton showering have been modeled using the Herwig generator. Moreover, the calculated cross-section of the $t\bar{t}$ signal multiplied by the branching ratio and filter efficiency(FE) in the ATLAS experiment is 90.54pb[32]. The description of same details for the background MC samples is tabled in Appendix A.

### 6.6.2 *Background*

There are several processes in the standard model with smaller cross-sections than the $t\bar{t}$ cross-section and produce one or more electron or muon in their final states. Hence, in addition to all the original signal leptons that are produced, there are also some *background* or non-signal leptons. In this analysis, all of the background events are obtained from applying the event selection cuts on the MC samples. Here is the list of the processes which produce at least one lepton that can be the background of the main $t\bar{t}$ events:

- **Single top quark**: Single top quark with comparable cross-section with the $t\bar{t}$ production is one of the important background of the top quark pair. Based on the branching ratio of about 100% the single top quark in this process decays to W-boson and b-quark and it is very close

to the state of the top quark pair process. The considerable difference between these two processes is the number of produced jets which in the case of single top quark is smaller than the number of them in the top quark pair processes. It increases the likelihood that background with high jet multiplicity like W+jets and QCD multi-jets dominate and makes it difficult to find out the original top quark signal in the single top quark events[45].

- **W + jets**: As it is shown in some samples of W+jets in Fig.18, the production of this event is similar to the $t\bar{t}$ semi-leptonic decays. W-boson decays to a lepton which is electron or muon and a lepton neutrino that contributes in missing transverse energy. Since this process is involved with jets, it is the important source for fake leptons in $t\bar{t}$ final states.

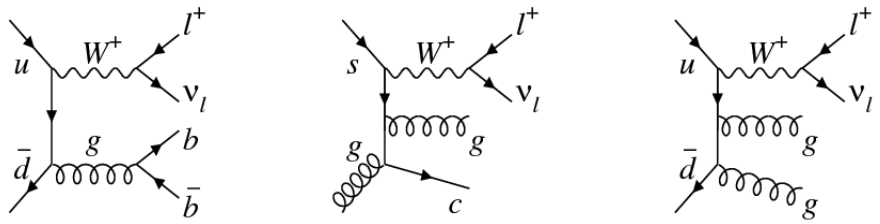


Figur 18: Some representative diagrams of W+jets production[42].

- **Dibosons**: Dibosons are usually presented by WW, ZZ and WZ processes. The diagrams are displayed in Fig.19. The result of the leptonic decay that can happen by all three forms, is a lepton and a lepton-neutrino which is taken into account as the missing transverse energy in the event.

- **Z-boson decays to tau leptons** ($Z \to \tau\tau$): This process is in electroweak scale and also occurs in hadronic scattering. The production of this process is the second highest background of the top quark pair decay. The final result of the tau leptons decay in this process is four leptons, two leptons that can be electron or muon and the two neutrinos. They are good reasonable evidence for being in the background of the top quark pair event.

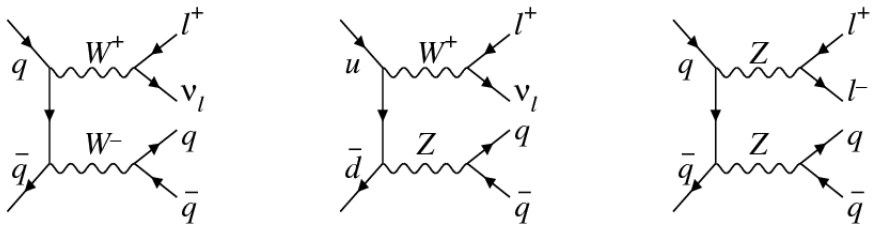


Figur 19: Feynman diagrams for diboson production (WW, WZ, ZZ)[42].

The final signal leptons must be reconstructed before being analyzed by their momentum four-vectors to model the top quark pair in the analysis. The result of the reconstruction process on the signal leptons is based on the detector and software with imperfections and the reconstruction efficiency which depends on the definition of the final leptons in the analysis. When the reconstruction process is not as perfect as it should be and the result is the object which is not produced like a signal lepton but can be reconstructed as a lepton; fake leptons come into account.
Even though the number of fake leptons in $t\bar{t}$ events are high due to the b-quark jet production, the ability of detector and reconstruction softwares to recognize the fake and signal leptons are remarkably high. It should also be considered that the detector and the softwares have a disability in identifying the initial parton of the objects in the jets. Hence, the uncertainty in finding the source of the fake leptons creates another problem in the modeling of an event. In the $t\bar{t}$ events, since electrons can be produced simply in most of the interactions, this misidentification affects mostly the electrons. Thus the explicit result cannot be given as it is seemed. One of the solutions for calculating the number of fake leptons is using a data driven method which is called the *Matrix Method*. Calculating the components of this matrix based on the fake leptons is a complicated process. Estimating the number of fake leptons are not included in this thesis but the short review is given.

## 6.7 *Matrix Method*

The matrix data driven method basically deals with the number of events containing fake leptons passing the selection criteria[35] and starts with two categories of definitions, the number of loose(l) and tight(t) events in data samples. Here, the concepts of loose and tight are different from those that are used to identify the leptons at object identification requirements. These

differences rise from the concepts of loose and tight selection requirements for selecting the analysis leptons in the event and the loose and tight selection cuts for the events in the method. In this method, as it is shown in

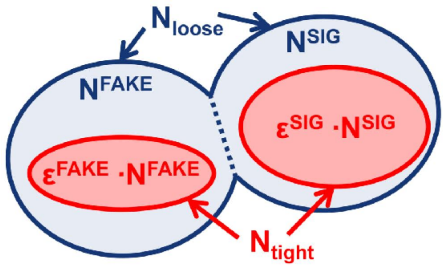


Figur 20: An illustration of the Matrix Method and the effect of the applied selection on the underlying sample subsets.[43]

Fig.20 the number of loose events before applying the event selection requirements is given by the summation of the number of signal and background contributions, the background is also called the fake"contribution.

$$N_{loose} = N^{sig} + N^{fake} \tag{16}$$

The number of tight events, after applying the defined selection requirements on the events, is the summation of the number of signal and fake tight events with the combination of the *fake rate(f)* and *real efficiency(r)* values. The result is written as:

$$N_{tight} = rN^{sig} + fN^{fake} \tag{17}$$

The fake rate is the probability of a loose fake lepton to satisfy the tight lepton selection requirements and the real efficiency is the probability of a loose real(signal) lepton, to be reconstructed as a tight lepton:

$$f = \frac{N^t_{fake}}{N^l_{Fake}} \tag{18}$$

$$r = \frac{N^t_{real}}{N^l_{real}} \tag{19}$$

In these equations $N^t_{fake}$ is the number of loose fake leptons which fulfill the tight lepton requirements, $N^l_{fake}$ is the number of loose fake leptons. $N^t_{real}$ is the number of loose real leptons that fulfill the tight lepton selection requirements and $N^l_{real}$ is the number of loose real leptons in the event. The

whole equation of this method in case of a dilepton decay when there are two leptons at the final state, can be written as:

$$\begin{pmatrix} N^{tt} \\ N^{tl} \\ N^{lt} \\ N^{ll} \end{pmatrix} = \begin{pmatrix} r_1 r_2 & r_1 f_2 & f_1 r_2 & f_1 f_2 \\ r_1(1-r_2) & r_1(1-f_2) & f_1(1-r_2) & f_1(1-f_2) \\ (1-r_1)r_2 & (1-r_1)f_2 & (1-f_1)r_2 & (1-f_1)f_2 \\ (1-r_1)(1-r_2) & (1-r_1)(1-f_2) & (1-f_1)(1-r_2) & (1-f_1)(1-f_2) \end{pmatrix} \begin{pmatrix} N^{ll}_{rr} \\ N^{ll}_{rf} \\ N^{ll}_{fr} \\ N^{ll}_{ff} \end{pmatrix} \tag{20}$$

The right column matrix is the number of selected events with two loose or tight leptons in the data, it yields this number for four different states of the final leptons. The middle matrix is the combination of calculations on real efficiency and fake rate in form of a 4 x 4 matrix. The indices 1 and 2 refers to the first and the second lepton, in fact to the electron and the muon in our case. The last right matrix represents four numbers of loose real or fake leptons before the event cut applying. Those variables which makes this calculation a bit complicated are fake rates and real efficiencies which are variant. These variables are dependent on the quantities of the properties like $P_t$ or $\eta$ of the leptons. The object quantities of fake leptons which comes up mostly from misidentified jet leptons in dileptonic decays, make the measurement accuracy over the fake rate and real efficiency harder. It should be mentioned that the sheer number of entries that are needed to be estimated is so large, the number of jets at each event is not clear and there are alot of other objects in each jet that cannot be recognized easily by the observer equipments and softwares. Therefore, this background is only included in the form of MC, in this study, known to be underestimated.

# 7 The Event Yields And Results

The overview of this analysis after finding the signal, data and background events, starts with subtracting the background from the data and comparing the results to the MC signal. The comparison between the background-subtracted data and the MC signal, as it was explained in the first chapter, is focused on some sensitive kinematic properties to the charge asymmetry in the final leptons and the simulated top quark pairs, like pseudorapidity and rapidity. The obtained overall number of expected events from the signal and data, after all the corrections and normalizations are shown in electron-muon channel and listed in the Table.2.

Having the final objects gives this opportunity to simulate the top quark pair mass in the events. The $t\bar{t}$ momentum value, according to the energy conservation law, before and after decay is conserved. The summation of momentum four-vector of the two leptons(e,$\mu$), missing transverse energy and at least two jets in both MC signal and data, in form of $t\bar{t}$ invariant mass, is obtained in Fig.21. As it is shown, signal and data are following the same shape. The peak of the distribution presents the mass of the top quark pair.

| **Channel** | **e$\mu$** |
|---|---|
| $t\bar{t}$ | 3390 $\pm$ 10 |
| Single Top | 162 $\pm$ 4 |
| Z $\rightarrow \tau\tau$ | 11 $\pm$ 1 |
| Dibosons | 4 $\pm$ 0.35 |
| W + jets | 1 $\pm$ 1 |
| Total | 3568 $\pm$ 16 |
| Data | 4899 |

Tabell 2: Obtained number of events in comparison to the expected number of signal and background contributions. The statistical uncertainties on the MC normalization are shown.

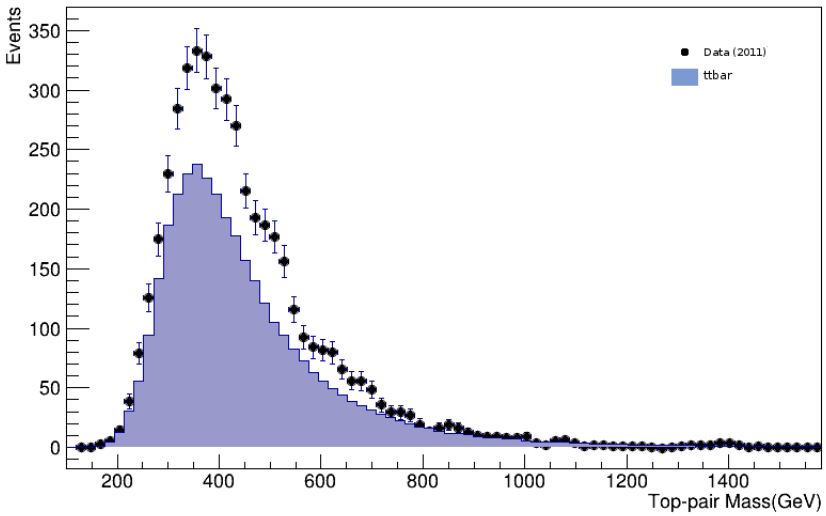


Figur 21: The selected top pair invariant mass distribution. The signal is $t\bar{t}$ MC sample and the data is background-subtracted. The MC signal is normalized and the data uncertainties are statistical.

It is approximately $m_{t\bar{t}} \simeq 350GeV$. After the peak region, due to the reduced efficiency of the fake leptons on the events around the tail, the distribution declines gradually. The number of fake leptons decreases in higher momentums.

The selection cuts on the transverse momentum on all of the top pair components in the Fig.22a has excluded alot of events around $P_t = 0$ and has made a sharp growth at the first part of the distribution. Fig.22b, represents the transverse energy. As much as the energy is higher the tail of the transverse energy is longer since the probability of finding a parton with the given energy decreases with the energy. Here also the simulation and data have the same similarities. This consistency of the distributions are also in the background as well as the signal and data. The different backgrounds of this study are shown in the Fig.23 separately.

As the background distributions show, the single top quark events have the majority of the backgrounds then Z$\rightarrow \tau\tau$ and dibosons respectively have the largest values and W + jets is the last and the ignorable case. All the distributions have mostly similar shape and the peaks of the plots in various backgrounds are very close to the one in the top quark pair distribution. Nevertheless, this arrangement in comparing with the most official background distributions of the year 2011 with $\sqrt{s} = 7TeV$, presents the other results. The official results of the year 2011 is shown in the Table.3.

| **Channel** | **e$\mu$** |
|---|---|
| $t\bar{t}$ | 4400 ± 500 |
| Single Top | 230 ± 20 |
| Z $\rightarrow \tau\tau$ | 180 ± 60 |
| Dibosons | 70 ± 4 |
| Multijets/W+jets | 250 ± 130 |
| Total | 5100 ± 500 |
| Data | 5305 |

Tabell 3: Official observed number of data events in comparison to the expected number of signal events and background contributions,at 2011. The statistical uncertainties on the MC normalization are shown [32].

The official results indicate W+jets as the most important background when in this analysis it is ignored since there is a huge uncertainty. This disagreement also is clear in the values of the other backgrounds.

In general there might be several reasons for this mismatching. One is the

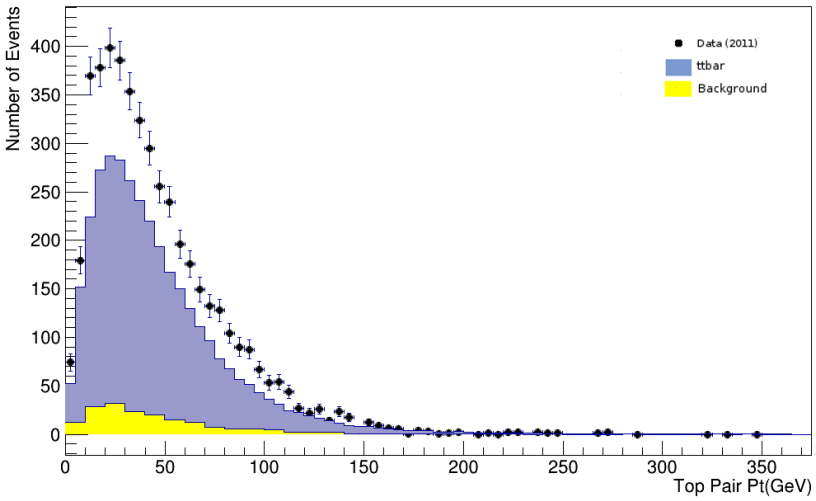


(a)

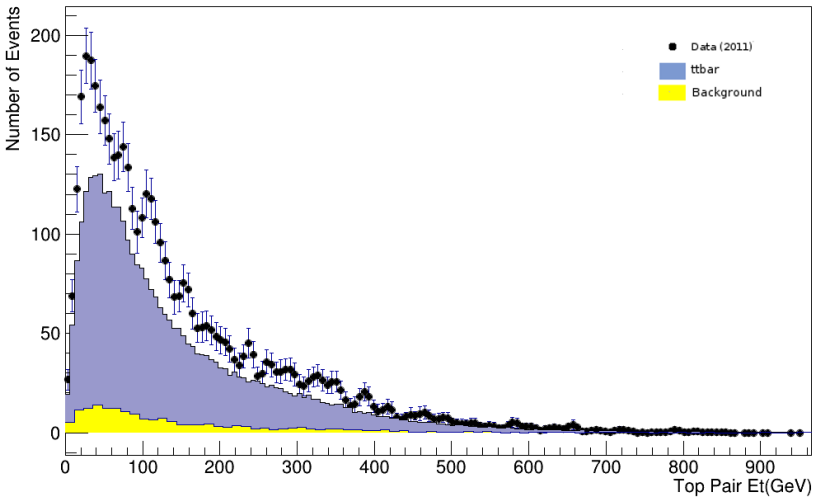


(b)

Figur 22: (a): The distribution of the selected top quark pair transverse momentum. (b): The distribution of the selected top quark pair transverse energy. The MC signal and the background in both distributions are normalized and the data uncertainties are statistical.

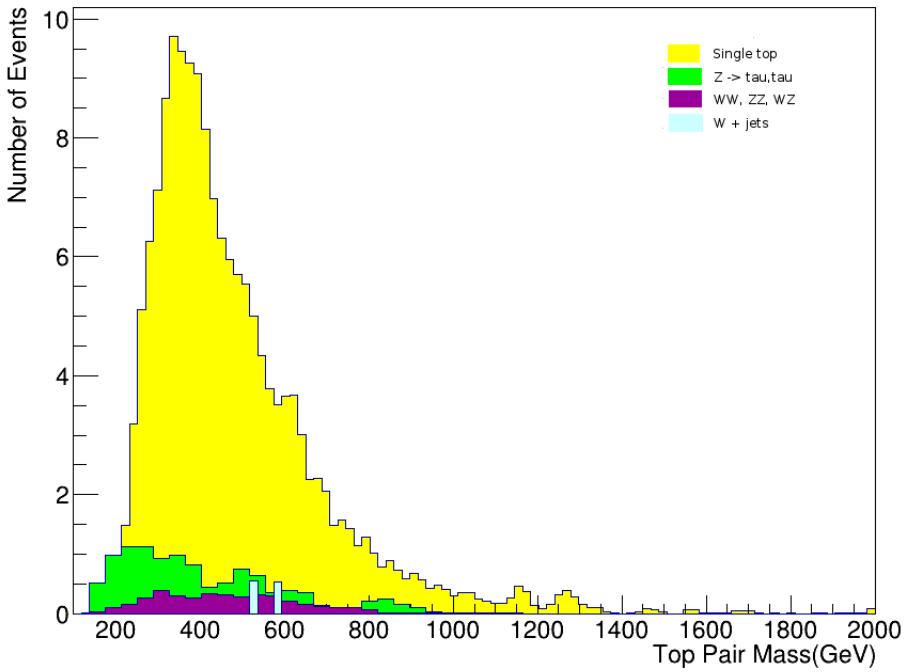


Figur 23: The distribution of $t\bar{t}$ event background in more details. The signal and the background are normalized and uncertainties are statistical.

fact that simulating some of these processes are very hard as they need a large number of events to make a reliable simulation. Some of these estimations also have a large statistical uncertainties and are hard to validate. Specifically in case of the W+jets, it is so rare to find a top quark pair in MC samples. Therefore, the obtained background and the fake leptons are yielded by data-driven method when in this study, the obtained number of event which is very tiny, comes from MC samples and no fake lepton has been measured. The obvious issue in comparing these two tables is the sequence of the other backgrounds that obeys the official results, although they have smaller quantities.

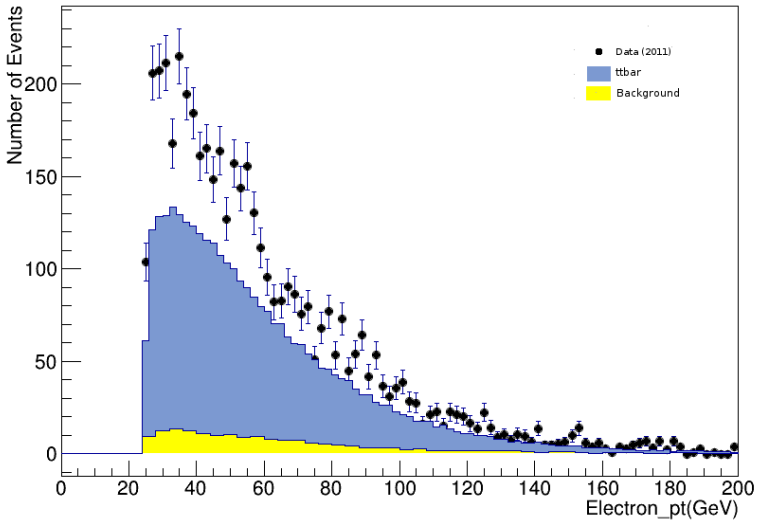


(a)

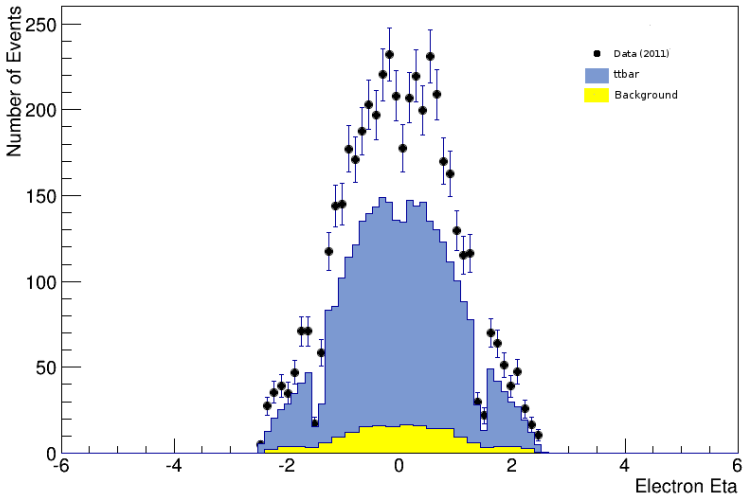


(b)

Figur 24: (a): The distribution of the selected electrons transverse momentum. (b): The distribution of the selected electrons pseudorapidity. The MC signal and the background in both distributions are normalized and the data uncertainties are statistical.

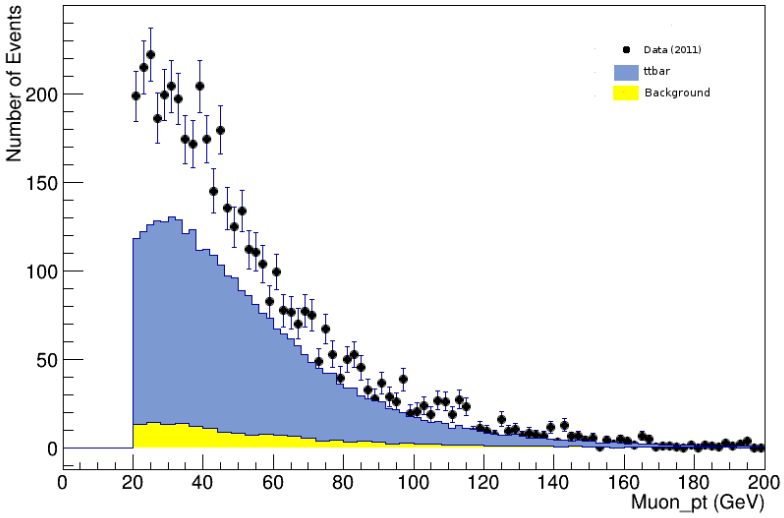


(a)

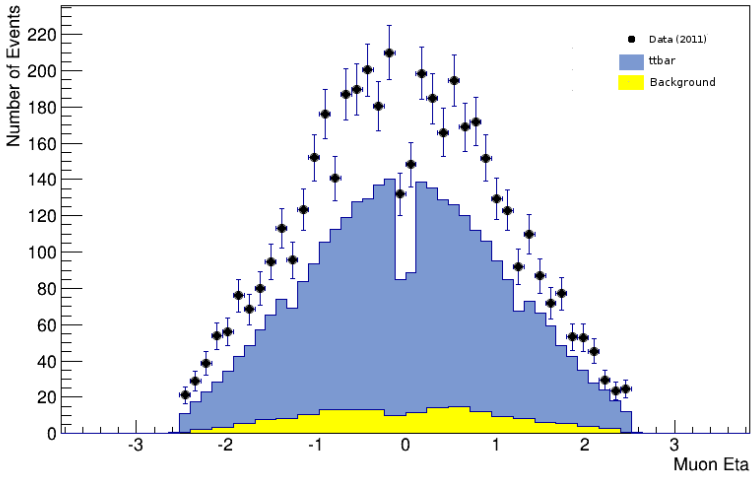


(b)

Figur 25: (a): The distribution of the selected muons transverse momentum. (b): The distribution of the selected muons pseudorapidity. The MC signal and the background in both distributions are normalized and the data uncertainties are statistical.

The electron kinematic property distributions are displayed in Fig.24a. The transverse of momentum starts from 25 GeV as it is determined in the momentum selection cut. The peak of the distribution shows the average maximum number of electrons is between 25 GeV to 40 GeV and then it has an exponential decay which represents there are just a few high energy electrons in whole the events. At lower momentums, there might be more fake electrons that mostly come from the misidentified jet objects.

The angular properties of the electron, electron pseudorapidity($\eta$) is shown in the Fig.24b. The distribution has covered the inner detector region between $|\eta_{cl}| < 2.5$ and the empty excluded criteria of the electron $\eta$ in the lepton selection cut which is at $1.37 < |\eta| < 1.52$ is clearly visible. Since the $t\bar{t}$ is supposed to be in the center, the peak of this distribution is seen in the center where the $t\bar{t}$ is produced. The signal and data in this plot are compatible and background is also in same state.

The kinematic properties of the muons is indicated in the Fig.25a and Fig.25b. The first figure, displays the momentum of muons. The distribution has same shape as the electron momentum distribution. Fake muons as the second possible misidentified leptons in this study are included in this distribution. They usually come from heavy-flavor contributions above 10 GeV. The started muon momentum value is set at 25 GeV. This cut rejects a large number of fake muons. The peak and the descend of the plot is similar to the electrons. The simulation of muons pseudorapidity in the Fig.25b covers the region of $|\eta| < 2.5$ as it should. Since there is no excluding region in this muon $\eta$, there is a difference between the shape of $\eta$ distribution and the electrons. Since there is no detector at $\eta = 0$, the muons cannot be reconstructed at this point and a gap at $\eta = 0$ is seen in the peak of the distribution.

The predicted estimation on the $t\bar{t}$ simulation in the Fig.26a indicates that a large multiplicity of high energetic jets in the top pair decay come from the momentum range between 25-100 GeV. There is also a good description in the obtained results and Fig.26b, the official results. The peaks of this distribution implies that the highest number of jets have the momentum about 50 GeV.

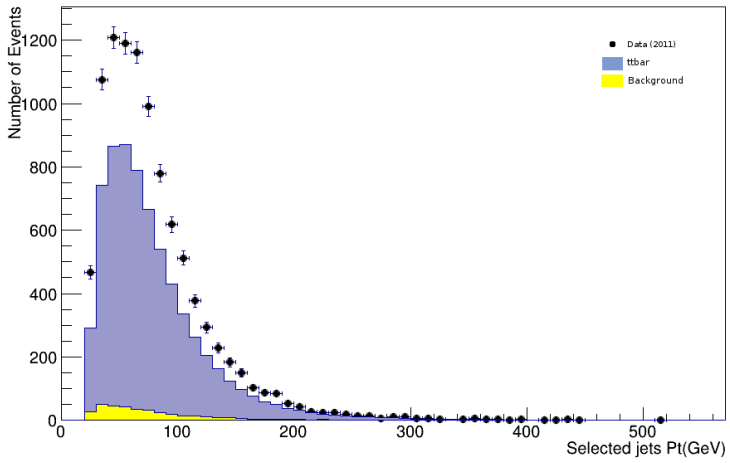


(a)

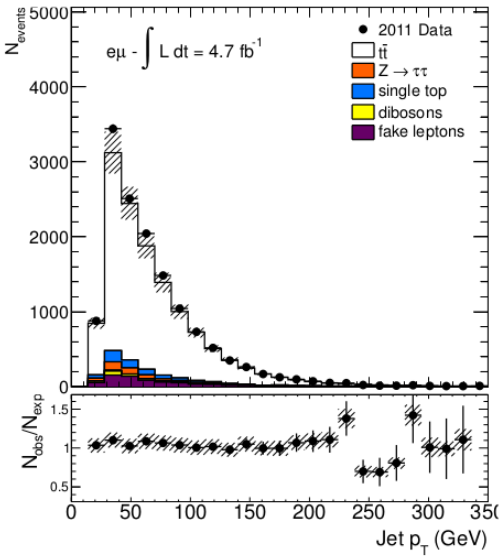


(b)

Figur 26: (a): The distribution of the momentum of the selected jets. The MC signal and the background in both distributions are normalized and the data uncertainties are statistical. (b): Data-MC comparisons of the selected jets momentums after selection in $e\mu$ channel from official results of 2011. Only statistical errors are taken into account. The shaded area shows the uncertainty on the signal and background normalization [32].

The other variable distributions of the event like the missing transverse energy and $H_t$ variable are also presented in Fig.27 and Fig.28. Due to the presence of the neutrinos and sometimes fake missing energy which comes up from the mis-measurement of the jet energies in the event, the tail of the missing transverse energy (MET) distribution is large at high values. In case of the $H_t$ value it can be said that it represents the momentum of the almost all of the involved particles of the top quark pair event. Therefore, as much as the energy of an event is higher and the heavier particles are produced, $H_t$ value shows more larger value and with higher probability it is the top quark pair included event.

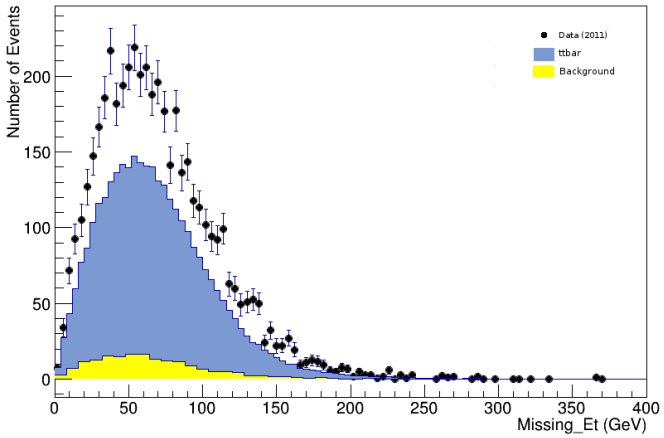


(a)

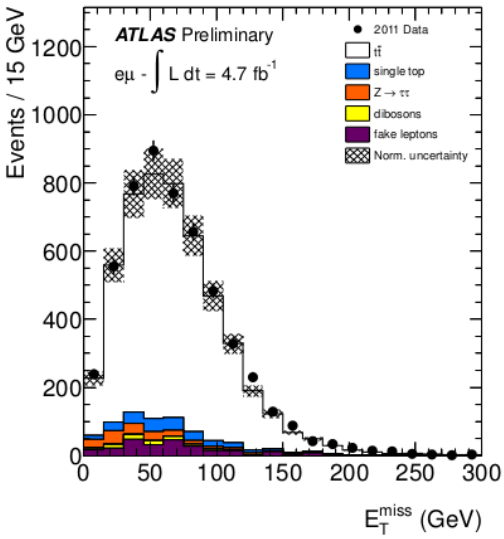


(b)

Figur 27: (a): The distribution of the missing transverse energy of the selected events. The MC signal and the background in both distributions are normalized and the data uncertainties are statistical. (b): Data-MC comparisons of the selectd events missing transverse energy after selection in $e\mu$ channel from official results of 2011. Only statistical errors are taken into account. The shaded area shows the uncertainty on the signal and background normalization [32].

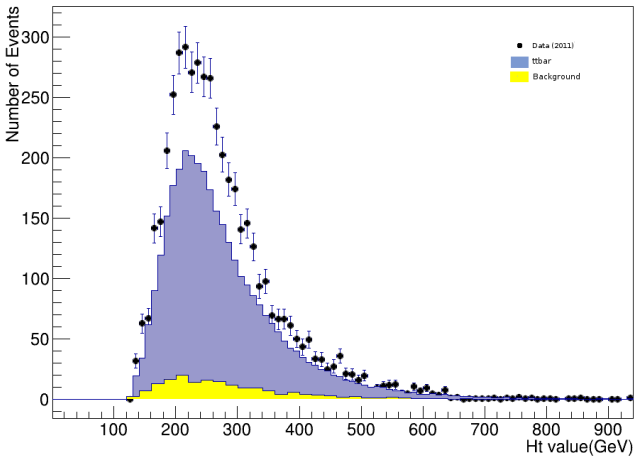


(a)

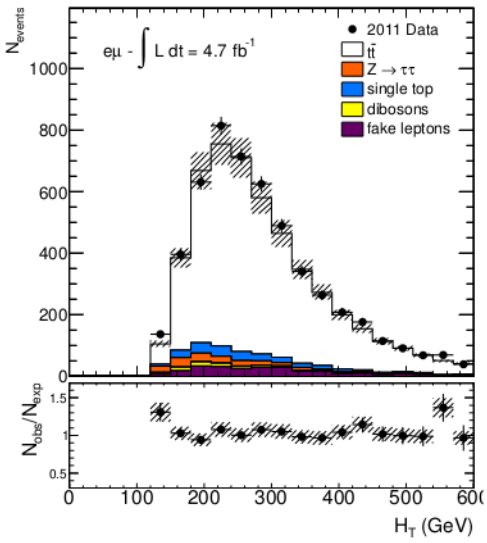


(b)

Figur 28: (a): The distribution of $H_t$ variable after event selection. The MC signal and the background in both distributions are normalized and the data uncertainties are statistical. (b): Data-MC comparisons of the $H_t$ variable after event selection in $e\mu$ channel from official results for year 2011. Only statistical errors are taken into account. The shaded area shows the uncertainty on the signal and background normalization [32].

## 7.1 *The Charge Asymmetry*

As it was explained in the first chapter, the charge asymmetry is calculable by two variables of pseudorapidity and rapidity. The data distribution is background-subtracted and the backgrounds are estimated on the MC samples. Here both $t\bar{t}$-based and leptonic-based charge asymmetry is calculated.

### 7.1.1 *The $t\bar{t}$-Based Charge Asymmetry Results*

Rapidity is the variable which is investigated for measuring the $t\bar{t}$-based charge asymmetry. The calculation of $t\bar{t}$-based charge asymmetry on both signal and data, according to the equation Eq.8, requires the difference value of the absolute rapidity of the top and anti-top quark. The estimated signal and background distribution of $\Delta|y| = |y_t| - |y_{\bar{t}}|$, for the top quark pair are presented in Fig.29 in the $e\mu$ channel. Since the rapidity is the combination

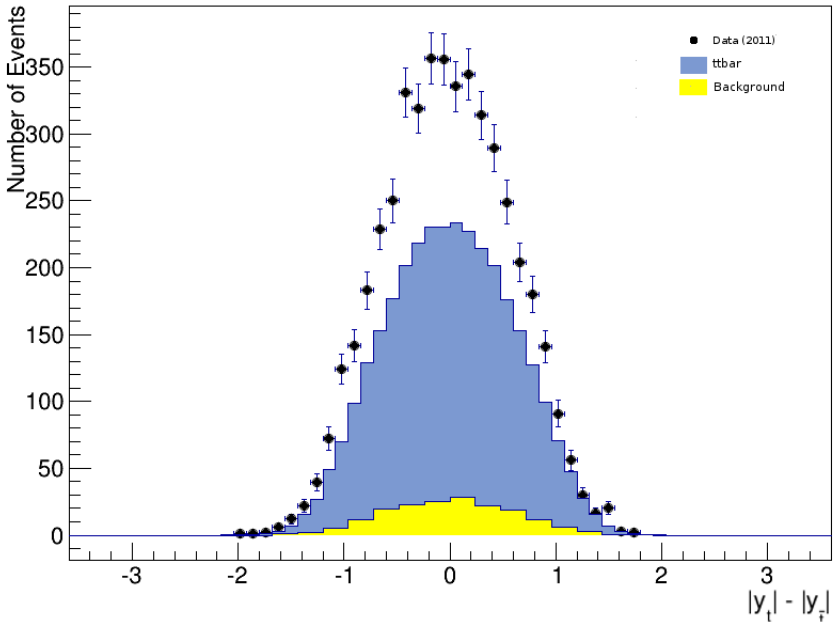


Figur 29: The distribution of the $\Delta|Y|$ for the selected top quark pairs in the $e\mu$ channel. The MC signal and the background in both distributions are normalized and the data uncertainties are statistical.

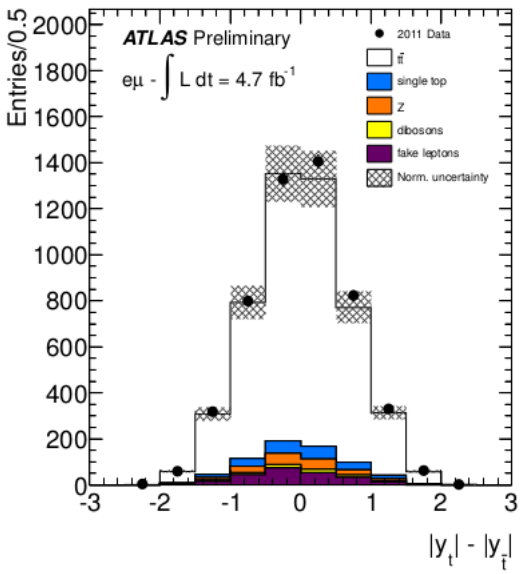


Figur 30: The official measured $\Delta|Y|$ distribution in year 2011 for the selected top quark pairs in the $e\mu$ channel. The shaded area represents the systematic uncertainties on the signal and background normalization[32].

of the energy and momentum natural logarithm, the distribution is supposed to cover the region between -2.7 to 2.7 which is shown in the related figure. Here the signal and the data are in same shape which is comparable with the official result in Fig.30. The positive and negative number of $\Delta|y|$, the final calculation of the $A_{t\bar{t}}^{C}$ in both MC and data is given in the Table.4. The official final results are tabled in Table.5.

The results in the Table.4 show that the absolute value of the positive rapidity is very close to the negative one that makes a very negligible difference in the formula and yields a very small value in the caclulation of the MC simulation charge asymmetry. This tiny difference value has a very large uncertainty which implies that there might be a large number of fake leptons or misidentified objects in the processes. Although in both cases, the final $t\bar{t}$-based symmetry show no asymmetry confirmation. The obtained values of data for $t\bar{t}$-based symmetry is in close agreement with the MC simulated signal.

| | $\mathbf{N}(\Delta\|y\| > 0)$ | $\mathbf{N}(\Delta\|y\| < 0)$ | **Charge asymmetry** |
|---|---|---|---|
| **MC** $t\bar{t}$ | 1695 ± 7 | 1697 ± 7 | -0.00058 ± 0.0029(stat.) |
| **Data** $t\bar{t}$ | 2276 ± 48 | 2446 ± 49 | -0.036 ± 0.0145(stat.) |

Tabell 4: The table presents the positive and negative number of $\Delta|y|$ and the measured $t\bar{t}$-based asymmetry values for the $e\mu$ channel in the MC, the data after the background subtraction, and related statistical uncertainties.

| | **Charge asymmetry** |
|---|---|
| **MC** $t\bar{t}$ | 0.006 ± 0.002(stat.) |
| **Data** $t\bar{t}$ | 0.037 ± 0.014(stat.) |

Tabell 5: The official measured $t\bar{t}$-based asymmetry values in year 2011, for the $e\mu$ channel and after the background subtraction only[32].

### 7.1.2 *Lepton-Based Charge Asymmetry Results*

For measuring the lepton-based charge asymmetry the sensitive variable, based on the Eq.9, is pseudorapidity. The pseudorapidity depends on the angle between momentum of the particle and the beam axis. The absolute value of this parameter covers the values less than 2.5 in the object selection cut. The difference value of the absolute pseudorapidities of the lepton pair, $\Delta|\eta| = |\eta_{l^+}| - |\eta_{l^-}|$, in $e\mu$ channel is plotted on both MC signal and data in the Fig.31. The comparable official plot is displayed the Fig.32.

The number of both positive and negative $\Delta|\eta|$ and the calculated lepton-based charge asymmetry, $A_{ll}^{C}$, results in both simulation and data are presented in Table.6 and is compared with the official results of 2011 in Table.7.

| | $\mathbf{N}(\Delta\|\eta\| > 0)$ | $\mathbf{N}(\Delta\|\eta\| < 0)$ | **Charge asymmetry** |
|---|---|---|---|
| **MC** $t\bar{t}$ | 1707 ± 7 | 1685 ± 7 | 0.006 ± 0.0029(stat.) |
| **Data** $t\bar{t}$ | 2378 ± 49 | 2384 ± 48 | 0.007 ± 0.014(stat.) |

Tabell 6: The positive and negative number of $\Delta|\eta|$ and the measured lepton-based asymmetry values for the $e\mu$ channel. The MC signal, the data after background subtraction and the related statistical uncertainties.

The results on both MC simulations are almost very close. However, the uncertainty still shows a very high value in comparison with the obtained

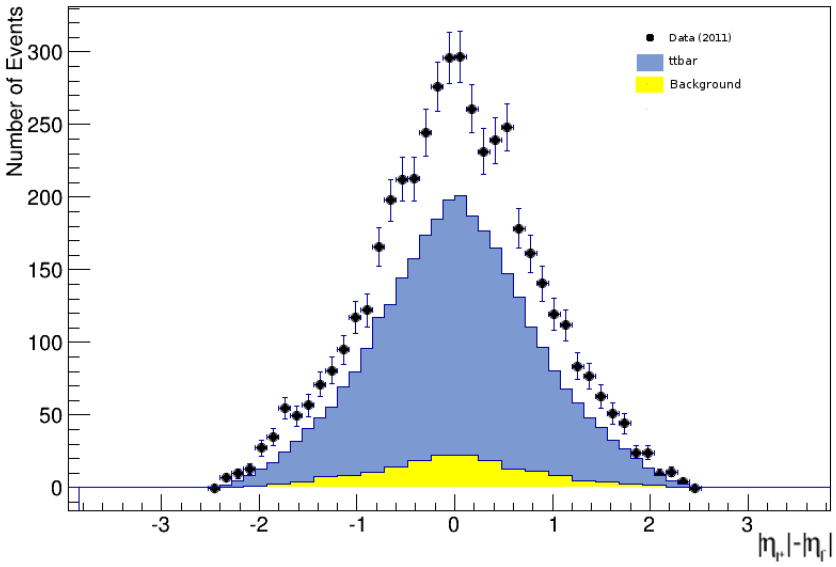


Figur 31: The distribution of the $\Delta|\eta|$ for selected lepton pairs in the $e\mu$ channel. The MC signal and background in both distributions are normalized and the data uncertainties are statistical.

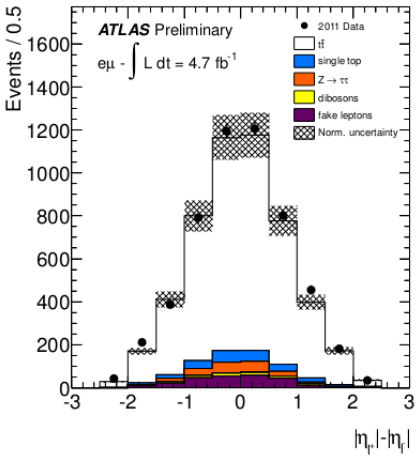


Figur 32: The official measured $\Delta|\eta|$ distribution of the year 2011 for selected lepton pairs in the $e\mu$ channel. The shaded area represents the systematic uncertainties on the signal and background normalization[32].

| | **Charge asymmetry** |
|---|---|
| **MC** $t\bar{t}$ | $0.004 \pm 0.001$(stat.) |
| **Data** $t\bar{t}$ | $0.019 \pm 0.017$(stat.) |

Tabell 7: The official measured lepton-based asymmetry values in 2011, for the (e,$\mu$) channel and after the background subtraction only[32].

asymmetry value. These measurements on data are also comparable, even with the high uncertainties which implies some deviations in the event selection criteria.

## 7.2 *Systematic Uncertainties*

There are several complicated effects in the experiment which raise from the sources like the detector modeling or the signal and background simulations. These effects can create the amount of uncertainties on the final measurements and should be taken into account as well as the statistical uncertainties for the final results. In this thesis, the systematic uncertainties of the experiment have been taken from the official values and are listed in the Table.8 and Table.9. Here is the brief explanation about the main contents of the tables:

- **ISR and FSR**: The uncertainty of the radiated gluons from the produced particles before hard collision in the $t\bar{t}$ events which is called *initial state radiation*, or ISR, and those gluons which are radiated from the final particles and are called the *final state radiation*, or FSR. Based on the energy of the initial and final radiations, an amount of uncertainty come into account to the measurements. If ISR and FSR are energetic radiation, an extra jet can be produced that causes a misidentification with any of the partons of the main event. The consequence of this misidentification, comes up in the population of the jets and the selection efficiency.

- **PDF**: The uncertainty of the parton distribution function or PDF which influences directly on the cross-section measurement.

- **JER and JES**: The uncertainties related to the reconstructing of the jets, light and b-jets. It is based on the difference in resolution on data and simulation. It affects the jet recognizing in the events and

jet finding efficiency. To remove this resolution gap, the JER and JES correction are applied on both model and data and the uncertainties in both correction processes are systematic. This uncertainty of JER is measured in data and is about 6% to 15%[32] based on jet momentum and pseudorapidity. This uncertainty of JES, in the center of region, is between 2.5% to 8%[32] and is dependent on jet $\eta$ and $P_t$.

- **Lepton efficiency and resolution**: This uncertainty is due to the difference in resolution of the final lepton identification in the model and data. Smearing the model can re-scale the lepton identification and make it match the data. This re-scaling contains statistical and systematic uncertainties.

- **Luminosity**: The luminosity is calculated and has systematic uncertainty. The uncertainty of the luminosity is about 3.9%[32] for this set of runs.

| | **e$\mu$ channel** |
|---|---|
| **Signal and background modeling** | |
| Signal generator | 0.003 |
| ISR and FSR | 0.004 |
| Parton showering/fragmentation | 0.004 |
| PDF | <0.001 |
| Z+jets | 0.004 |
| Dibosons | <0.001 |
| Single top | <0.001 |
| Multijet background | 0.002 |
| **Detector modeling** | |
| Jet efficiency and resolution(JER) | 0.001 |
| Jet energy Scale(JES) | 0.001 |
| Muon efficiency and resolution | 0.001 |
| Electron efficiency and resolution | 0.003 |
| Calibration | 0.002 |
| Luminosity | <0.001 |
| Total | 0.009 |

Tabell 8: The list of all systematic uncertainties on the lepton-based asymmetry[32].

| | **e$\mu$ channel** |
|---|---|
| **Signal and background modeling** | |
| Signal generator | 0.003 |
| ISR and FSR | 0.004 |
| Parton showering/fragmentation | 0.004 |
| PDF | <0.001 |
| Z+jets | 0.004 |
| Dibosons | <0.001 |
| Single top | <0.001 |
| Multijet background | 0.002 |
| **Detector modeling** | |
| Jet efficiency and resolution | 0.001 |
| Jet energy Scale | 0.001 |
| Muon efficiency and resolution | 0.001 |
| Electron efficiency and resolution | 0.003 |
| Calibration | 0.002 |
| Luminosity | <0.001 |
| Total | 0.009 |

Tabell 9: The list of all systematic uncertainties on the $t\bar{t}$-based asymmetry[32].

# 8 Conclusion

This thesis studied the measurement of the charge asymmetry in top quark pair decay in dilepton (e,$\mu$) channel in pp collision data at the center of mass energy of $\sqrt{s} = 7TeV$ corresponding to an integrated luminosity of $4.58fb^{-1}$ and the data are taken by the ATLAS experiment. The charge asymmetry in the top quark pair observed at Tevatron in Fermilab for the first time. In this accelerator, the collision beams are proton and anti-proton and the measurement of the asymmetry is based on the top quarks produced in the direction of the proton/anti-proton beam.
At the ATLAS detector, where both of the collision beams are protons, the charge asymmetry is measured based on two methods of $t\bar{t}$-based and lepton-based in the top quark pair events that are configured by two leptons, one electron and one muon, a missing transverse energy and at leas two jets at the final state. The experiment has several backgrounds. The background of this study consists of single top quarks, Z $\rightarrow \tau\tau$, dibosons and W+jets. All of the backgrounds are simulated on the MC samples and the MC samples are from MC@NLO, next-to-leading-order QCD event generator. To reconstruct the top and anti-top quark events various particles in the events should pass the object selection criteria and be chosen as the final particle to be taken into account for the final distribution on the MC and the data. After the reconstruction on the $t\bar{t}$ MC samples and the backgrounds, the data is also distributed based on this reconstruction. After normalizing the MC simulation and the background, the background is subtracted from the data and the required variables are taken from the MC and data signals to be used in the asymmetry equations.

The $t\bar{t}$-based charge asymmetry is based on the rapidity differences between the top and anti-top quark. Calculating the difference between the positive and negative number of $\Delta|Y|$ on both MC simulation and data gives the related results of:

$$MC : A_{t\bar{t}}^{C} = -0.0005 \pm 0.0029(stat.)$$

$$Data : A_{t\bar{t}}^{C} = -0.036 \pm 0.0145(stat.)$$

when the official results of 2011 represents the same calculations as:

$$MC : A_{t\bar{t}}^{C} = 0.006 \pm 0.002(stat.)$$

$$Data : A_{t\bar{t}}^{C} = 0.037 \pm 0.014(stat.)$$

The second asymmetry measurement, the lepton-based charge asymmetry which concerns the pseudorapidity between the electron and the muon as the final leptons, yields the results on MC and data as:

$$MC : A_{ll}^{C} = 0.006 \pm 0.0029(stat.)$$

$$Data : A_{ll}^{C} = 0.007 \pm 0.014(stat.)$$

when the official results are:

$$MC : A_{ll}^{C} = 0.004 \pm 0.001(stat.)$$

$$Data : A_{ll}^{C} = 0.019 \pm 0.017(stat.)$$

Some of the values in this experiment do not show very close agreement with the official values or have very large uncertainties. It implies the existence of the large number of fake leptons or some deviations in event selections criteria in the analysis which is due to lack of access to the accurate documents for choosing the correct selection cuts. This regarding the previous reasons, all the obtained data values in the $t\bar{t}$-based asymmetry and the lepton-based asymmetry, with some uncertainty corrections, covers the MC simulations and are in a good agreement with the 2011 official results. It implies clearly that there is no evidence to break the physics of the Standard Model.

Some of the reasons of this mismatching might be solved if:

- The right object and event selection cuts are chosen.
- Measuring some of the backgrounds like multijets/W+jets by the data-driven method, matrix method.

- Considering the fake leptons in the simulation and background measurements.
- Bringing more details like data correction after the background subtracting, detector effects and the calibration into account.

It should also be considered that the C++ simulation program of this analysis has been written by the student and might involve more unknown bugs and mismatching than the official group might face to.

# 9 Appendix A

| ID | Description | Matrix Element | Parton Shower | cross section [pb] | $k$-factor |
|---|---|---|---|---|---|
| 5200 | $t\bar{t}$ No full hadr. $(e, \mu, \tau)$ | MC@NLO | Herwig | 79.01 | 1.146 |
| 8340 | tchan $\rightarrow e$ | MC@NLO | Herwig | 7.12 | 1 |
| 8341 | tchan $\rightarrow \mu$ | MC@NLO | Herwig | 7.12 | 1 |
| 8342 | tchan $\rightarrow \tau$ | MC@NLO | Herwig | 7.10 | 1 |
| 8343 | schan $\rightarrow e$ | MC@NLO | Herwig | 0.47 | 1 |
| 8344 | schan $\rightarrow \mu$ | MC@NLO | Herwig | 0.47 | 1 |
| 8345 | schan $\rightarrow \tau$ | MC@NLO | Herwig | 0.47 | 1 |
| 8346 | $Wt \rightarrow$ inclusive | MC@NLO | Herwig | 14.59 | 1 |

Figur 33: Top Monte-Carlo samples.[26]

| ID | Description | Matrix Element | Parton Shower | cross section [pb] | $k$-factor |
|---|---|---|---|---|---|
| 105985 | WW | Herwig | | 11.5003 | 1.48 |
| 105986 | ZZ | Herwig | | 0.9722 | 1.30 |
| 105987 | WZ | Herwig | | 3.4641 | 1.60 |

Figur 34: Diboson samples.[26]

| ID | Description | Matrix Element | Parton Shower | cross section [pb] | $k$-factor |
|---|---|---|---|---|---|
| 7670 | Ztautau Np0 | Alpgen | Herwig | 668.40 | 1.25 |
| 7671 | Ztautau Np1 | Alpgen | Herwig | 134.81 | 1.25 |
| 7672 | Ztautau Np2 | Alpgen | Herwig | 40.36 | 1.25 |
| 7673 | Ztautau Np3 | Alpgen | Herwig | 11.25 | 1.25 |
| 7674 | Ztautau Np4 | Alpgen | Herwig | 2.79 | 1.25 |
| 7675 | Ztautau Np5 | Alpgen | Herwig | 0.77 | 1.25 |

Figur 35: Z+jet samples with phase space cuts $m_{ll} > 40GeV$.[26]

| ID | Description | Matrix Method | Parton Shower | Cross-section[pb] | k-factor |
|---|---|---|---|---|---|
| 7680 | Wenu Np0 | Alpgen | Jimmy | 6930.5 | 1.196 |
| 7681 | Wenu Np1 | Alpgen | Jimmy | 1305.30 | 1.196 |
| 7682 | Wenu NP2 | Alpgen | Jimmy | 378.13 | 1.196 |
| 7683 | Wenu Np3 | Alpgen | Jimmy | 101.86 | 1.196 |
| 7684 | Wenu Np4 | Alpgen | Jimmy | 25.68 | 1.196 |
| 7685 | Wenu Np5 | Alpgen | Jimmy | 6.99 | 1.196 |

Tabell 10: Samples of W+jets when the final leptons are electron and el-neutrino.[44].

| ID | Description | Matrix Method | Parton Shower | Cross-section[pb] | k-factor |
|---|---|---|---|---|---|
| 7690 | Wmunu Np0 | Alpgen | Jimmy | 6932.4 | 1.195 |
| 7691 | Wmunu Np1 | Alpgen | Jimmy | 1305.90 | 1.195 |
| 7692 | Wmunu NP2 | Alpgen | Jimmy | 378.07 | 1.195 |
| 7693 | Wmunu Np3 | Alpgen | Jimmy | 101.85 | 1.195 |
| 7694 | Wmunu Np4 | Alpgen | Jimmy | 25.72 | 1.195 |
| 7695 | Wmunu Np5 | Alpgen | Jimmy | 7.00 | 1.195 |

Tabell 11: Samples of W+jets when the final leptons are muon and mu-neutrino.[44].

# 10 References


1. http://en.wikipedia.org/wiki/Standard_Model, This page was last modified on 14 November 2014 at 14:24.

2. S. Biswas, *Fermi-Dirac Statistics*. School of Physics, University of Hyderabad, (2014).

3. Jens Eisert, *Pauli Principle, Reloaded*. QMIO Group, Dahlem Center for Complex Quantum Systems, Freie Universität Berlin. *Physics 6, 8*, (2013).

4. Leif Jonnson, *Lecture of introduction to Elementary Particle Physics*, Lund University.

5. A. Pich. *The standard model of electroweak interactions*. Spires, hep-ph(0502010v1), (2007).

6. Y. A. Ceccucci (CERN), Z. Ligeti (LBNL), and Y. Sakai (KEK). *The CKM quark-mixing matrix*, (2012).

7. D0 Collaboration, *Observation of the Top Quark*, Phys. Rev. Lett. 74:2632-2637, hep-ex/9503003, (1995).

8. Frank-Peter Schilling, Top Quark Physics at the LHC: A Review of the First Two Years. Institute of Experimental Nuclear Physics (EKP), Karlsruhe Institute of Technology (KIT), D-76128 Karlsruhe, Germany, arXiv:1206.4484v1 [hep-ex], (2012).

9. J. Beringer et al. (Particle Data Group), PR D86, 010001. (2012) and (2013) partial update for the (2014) edition.

10. Baglio, Julien; Djouadi, Abdelhak *Higgs production at the LHC*. Journal of High Energy Physics 1103 (3): 055. arXiv:1012.0530v5 [hep-ph], (2011).

11. http://atlas-service-enews.web.cern.ch/atlas-service-enews/2007-8/features_07-8/features_wmass.php. Troels Petersen, *Measuring the W mass with ATLAS*, ATLAS e-News, (2011).

12. Hasegawa, Satoshi (Nagoya U.), Makoto, Tomoto (dir.) (Nagoya U.). *Measurement of the W boson polarization in top quark decays using the di-lepton final state of the top quark pair in pp collisions with p* $\sqrt{s}$*=7 TeV*, CERN-THESIS-2013-030, (2013).

13. J. Pumplin, D.R. Stump, J. Huston, H.L. Lai, P. Nadolsky, W.K. Tung, *New Generation of Parton Distributions with Uncertainties from Global QCD Analysis*. Journal of high energy physics, arXiv:hep-ph/0201195v3, (2002).

14. Heim, Sarah et al. *Next-to-leading order QCD corrections to s-channel single top quark production and decay at the LHC*, Phys.Rev. D81 (2010)034005. arXiv:0911.0620 [hep-ph] ANL-HEP-PR-09-94, EFI-09-22, MSUHEP-091025, (2010).

15. Wicke Daniel, *Properties of the top quark*, Eur.Phys.J. C71 (2011) 1627 arXiv:1005.2460 [hep-ex] FERMILAB-HABIL-2009-01, (2011).

16. A. Carmona, M. Chala, A. Falkowski, S. Khatibi, M. M.Najafabadi, G. Perez, J. Santiago. *From Tevatron's top and lepton-based asymmetries to the LHC*, CERN-PH-TH/2014-005, (2014).

17. J. O.Antunano and G. Rogdrigo, *Top quarks,axigluons and charge asymmetries at hadron colliders*, Phys. Rev. D77(2008)014003, (2008).

18. J. H. Kuhn and G. Rodrigo, *Charge asymmetry of heavy quarks at hadron colliders*, Phys. Rev. D 59, 054017, (1999).

19. Paul G. Schreier, *Sensors and Instrumentation Of the Superlative Class*. EE-Evaluation Engineering journal 200811, (2008).

20. Jacob Groth-Jensen, *Luminosity determination and simulation of the LUCID detector at the ATLAS experiment*, PhD thesis at Lund University, (2010).

21. The ATLAS Collaboration, *Liquid argon calorimeter technical design report*. CERN/LHCC/96-041, (1996).

22. The ATLAS Collaboration, *ATLAS Detector and physics performance technical design report*, CERN/LHCC/99-14, ATLAS TDR 14 25 MAY (1999).

23. http://www.fsp101-atlas.de/e197881/e200224/.

24. The ATLAS Collaboration, *The ATLAS trigger system*, Eur Phys J C 34, s01,s173-s183, (2004).

25. http://www.fysik.su.se/∼cohm/trigger.html.

26. J. Antos et al., *Measuring of the charge asymmetry in top quark pair dileptonic channel in pp collisions at* $\sqrt{s} = 7$ *TeV using the ATLAS detector*, ATLAS-CONF-2012-057 (supporting Documents), (2012).

27. The ATLAS Collaboration, *Electron performance measurements with the ATLAS detector using the 2010 LHC proton-proton collision data*, Eur. Phys. J. C, CERN-PH-EP-2011-117, (2012).

28. http://folk.uio.no/maikenp/pages/Work/phd/statush2010/page2/.

29. M. Cacciari, G. P. Salam and G. Soyez, JHEP 0804, 063(2008), *The anti-$k_t$ clustring algorithm*, arXiv:0802.1189[hep-ph], (2008).

30. E. Fernandez et al., *Lifetime of Particles Containing b Quarks*, Phys. Rev. Lett. 51, 1022, (1983).

31. https://twiki.cern.ch/twiki/bin/view/AtlasProtected/, *How To Clean Jets 2011*, (2011).

32. *Measurement of the charge asymmetry in top quark pair production in pp collision data at* $s = 7$ *TeV using the ATLAS detector*, ATLAS-CONF-2012-057, (2012).

33. S. Hassani, L. Chevalier, E. Lancon, J.-F. Laporte, R. Nicolaidou, A. Ouraou, *A muon identification and combined reconstruction procedure for the ATLAS detector at the LHC using the (MUONBOY, STACO, MuTag) reconstruction packages*, doi:10.1016/j.nima.2006.10.340, (2006).

34. V. Boisvert on behalf of the ATLAS Collaboration, *Top quarks objects definition and performance at ATLAS*, Journal of Physics: Conference Series 452(2013) 012012, (2013).

35. http://atlas-proj-computing-tdr.web.cern.ch/atlas-proj-computing-tdr/Html/ Computing-TDR-21.htm#pgfId-1019542. *The Athena Framework*, (2005).

36. http://root.cern.ch/drupal/content/about.

37. http://wlcg-public.web.cern.ch/.

38. P. Nason (INFN, Milan) and P.Z. Skands (CERN), *Monte Carlo event generators*, (2012).

39. S. Agostinelli et al., Geant4 – a simulation toolkit, *Nuclear Instruments and Methods in Physics Research Section A: Accelerators, Spectrometers, Detectors and Associated Equipment* Online journal Elsevier, Volume 506, Issue 3,(2003).

40. https://twiki.cern.ch/twiki/bin/viewauth/Atlas/GoodRunsListsTutorial.

41. Max Baak (CERN), *Good run lists, what about them*, ATLAS e-News (2011).

42. The CDF Collaboration, Altonen, T. et al.,*Search for Standard Model Higgs Boson Production in Association with a W Boson Using a Matrix Element Technique at CDF in pp Collisions at s=1.96 TeV*, Phys.Rev. D85 (2012) 072001, arXiv:1112.4358 [hep-ex], (2012).

43. Fabian Kohn,*Measurement of the charge asymmetry in top quark pair production in pp collision data at sqrt(s) = 7 TeV using the ATLAS detector*, PhD thesis, arXiv:1204.0952 [hep-ex], (2012).

44. https://twiki.cern.ch/twiki/bin/view/AtlasProtected/TopMC11#W_jets.

45. A. S. Belyaev, E. E. Boos, L. V. Dudko, *Single Top Quark at Future Hadron Colliders. Complete Signal and Background Study*, arXiv:hep-ph/9806332v5, (1999).